



1 Quantifying methane emissions from natural gas production in 2 northeastern Pennsylvania

3 Zachary R. Barkley¹, Thomas Lauvaux¹, Kenneth J. Davis¹, Aijun Deng¹, Yanni Cao¹, Colm Sweeney²,
4 Douglas Martins⁷, Natasha L. Miles¹, Scott J. Richardson¹, Thomas Murphy⁴, Guido Cervone⁵, Anna
5 Karion², Stefan Schwietzke⁸, MacKenzie Smith³, Eric A. Kort³, Joannes D. Maasakkers⁶

6 ¹Department of Meteorology, The Pennsylvania State University, University Park, PA 16802, United States

7 ²NOAA/Earth Systems Research Laboratory, University of Colorado, Boulder, CO, 80305, United States

8 ³Department of Climate and Space Sciences and Engineering, University of Michigan, Ann Arbor, MI, 48109, United States

9 ⁴Marcellus Center for Outreach and Research, The Pennsylvania State University, University Park, PA 16802, United States

10 ⁵Department of Geography, The Pennsylvania State University, University Park, PA 16802, United States

11 ⁶School of Engineering and Applied Sciences, Harvard University, Pierce Hall, 29 Oxford Street, Cambridge, Massachusetts
12 02138, United States

13 ⁷FLIR Systems, West Lafayette, IN 47906, United States

14 ⁸Cooperative Institute for Research in Environmental Sciences, University of Colorado, Boulder, Colorado, USA.

15

16

17 *Correspondence to:* Zachary R. Barkley (zrb5027@psu.edu)

18

19

20 **Abstract.** Natural gas infrastructure releases methane (CH₄), a potent greenhouse gas, into the atmosphere. The estimated
21 emission rate associated with the production and transportation of natural gas is uncertain, hindering our understanding of its
22 greenhouse footprint. This study presents a new application of inverse methodology for estimating regional emission rates
23 from natural gas production and gathering facilities in northeastern Pennsylvania. An inventory of CH₄ emissions was
24 compiled for major sources in Pennsylvania. This inventory served as input emission data for the Weather Research and
25 Forecasting model with chemistry enabled, and atmospheric CH₄ mole fraction fields were generated at 3km resolution.
26 Simulated atmospheric CH₄ enhancements from WRF-Chem were compared to observations obtained from a three-week flight
27 campaign in May 2015. Modelled enhancements from sources not associated with upstream natural gas processes were
28 assumed constant and known and therefore removed from the optimization procedure, creating a set of observed enhancements
29 from natural gas only. Simulated emission rates from unconventional production were then adjusted to minimize the mismatch
30 between aircraft observations and model-simulated mole fractions for ten flights. To evaluate the method, an aircraft mass
31 balance calculation was performed for four flights where conditions permitted its use. Using the model optimization approach,
32 the weighted mean emission rate from unconventional natural gas production and gathering facilities in northeastern
33 Pennsylvania approach is found to be 0.36% of total gas production, with a 2σ confidence interval between 0.27-0.45% of
34 production. Similarly, the mean emission estimates using the aircraft mass balance approach is calculated to be 0.34% of
35 regional natural gas production, with a 2σ confidence interval between 0.06-0.62% of production. These emission rates as a



36 percent of production are lower than rates found in any other basin using a top-down methodology, and may be indicative of
37 some characteristics of the basin that makes sources from the northeastern Marcellus region unique.

38 **1 Introduction**

39 The advent of hydraulic fracturing and horizontal drilling technology has opened up the potential to access vast reservoirs of
40 natural gas previously inaccessible, shifting energy trends in the United States away from coal and towards natural gas (EIA,
41 2016b). From a greenhouse gas (GHG) emissions perspective, natural gas has the potential to be a cleaner energy source than
42 coal. For every unit of energy produced, half as much carbon dioxide (CO_2) is emitted through the stationary combustion of
43 natural gas in comparison to coal (EPA, 2016). However, during the process of extracting and distributing natural gas a
44 percentage of the overall production escapes into the atmosphere through both planned releases and unintended leaks in
45 infrastructure. Though these emissions may be from an economic perspective, their climatological impacts are not negligible
46 (Alvarez et al., 2012; Schwietzke et al., 2014). Methane (CH_4), the main component of natural gas, is a potent greenhouse gas
47 with a global warming potential over a 20-year period (GWP_{20}) of 84 (Myhre et al., 2013). Over a 100-year period the GWP
48 is reduced to 28 due to interactions with the hydroxyl radical which transform the CH_4 molecule to CO_2 . Depending on which
49 timespan is used, the relative climatological impacts of natural gas as an energy source compared to coal can vary. Using the
50 GWP_{20} value, it is estimated that a natural gas emission rate of only 3% of total gas production would result in a natural gas
51 power plant having a more negative impact on the climate than a coal-powered plant. Using the GWP_{100} value, this emission
52 rate threshold shifts to 10% of production (Schwietzke et al., 2014; Alvarez et al., 2012). Complicating matters further, the
53 future climate impacts associated with an increased availability of natural gas extends well beyond a simple greenhouse gas
54 footprint comparison against coal. Lower fuel prices linked to this new reservoir of energy can change the course of future
55 energy development globally. With many states and countries attempting to find a suitable balance between their energy
56 policies and greenhouse gas footprint, it is important for the scientific community to be able to quantify and monitor natural
57 gas emission rates.

58 The mining and transfer of natural gas can be broken down into five stages: production, processing, storage,
59 transmission, and distribution. The Environmental Protection Agency (EPA) uses a bottom-up approach to quantify these
60 emissions, estimating emission rates per facility or component (such as a compressor, unit length of pipeline, pneumatic device)
61 or an average emission per event (such as a well completion or liquids unloading). These “emission factors” are then multiplied
62 by nationwide activity data containing the number of components or events associated with each emission factor, and a total
63 emission rate is produced for the country (EPA, 2015b). This bottom-up approach is a practical methodology for estimating
64 emissions over a large scale but has limitations. A bottom-up inventory depends on the quality and quantity its emission factors
65 and activity data. Emissions from sources in the natural gas industry can be temporally variable and have a wide range of
66 values depending on a number of factors, such as the quality and age of the device and the gas pressure moving through the
67 component. Furthermore, recent studies have shown that a majority of emissions comes from a small percentage of devices,



68 often referred to as “super-emitters”, creating a long-tail distribution of emission sources (Brandt et al., 2014, Omara et al.,
69 2016, Zavala-Araiza et al., 2015, 2017, Frankenberg et al., 2016). These two factors make it difficult to sample enough devices
70 and adequately describe the mean emission rate, thus allowing for significant representation errors in the emission factors.
71 Because emission factors are required for hundreds of different components, these errors can accumulate and lead to systematic
72 biases in the total emissions estimate.

73 One way to compare results based on inadequate sample sizes in the bottom-up approach is to measure the aggregated
74 enhancement in the atmospheric mole fraction at larger scales through a top-down approach. Instead of measuring emissions
75 from individual devices and scaling up, a top-down approach takes atmospheric greenhouse gas concentrations measured
76 downwind of a continent (e.g. Bousquet et al., 2006), a region (e.g. Lauvaux et al., 2008), a city (e.g. White et al., 1976, Mays
77 et al., 2009, Lamb et al., 2016) or a facility (e.g. Ryerson et al., 2001) and uses inverse methodologies to attribute the
78 enhancements to potential sources upwind. One of these methods, the aircraft mass balance technique, has been performed at
79 many different oil and gas fields to characterize natural gas emissions (Petron et al., 2012, Karion et al., 2013, 2015, Peischl
80 et al., 2015, Conley et al., 2016). While this methodology is able to capture surface fluxes over a large region, it remains
81 difficult to attribute the emissions to any individual source (Cambaliza et al., 2014). Any sources from within the flux region
82 that emit CH₄ will be measured in the downwind observations and be a part of the aggregated regional enhancement.
83 Atmospheric observations also include other sources unrelated to natural gas, such as anaerobic respiration from landfills and
84 wetlands, enteric fermentation from cattle, anaerobic decomposition of manure, CH₄ seepage from coal mining, and many
85 other smaller sources. If the purpose of the study is to solve for the emissions from the natural gas industry, emissions from all
86 sources unrelated to natural gas must be known and removed from the regional flux estimate. Thus, top-down experiments
87 require an accurate CH₄ inventory of the study area and any errors associated with the inventory will propagate into the final
88 emissions estimate. A more advanced technique to separate out non-natural gas sources has been developed using ethane as a
89 tracer for natural gas (Smith et al., 2015). However, such methods may struggle in dry gas basins where smaller ethane to
90 methane ratios within the gas can make the ethane signature more difficult to separate out. And similar to bottom-up methods,
91 top-down studies fail to address temporal variability, with observations from many of these studies having been collected
92 during a limited number of 2 to 4 hour aircraft flights performed over a period of weeks.

93 In recent years, both bottom-up and top-down studies have aimed at calculating natural gas emission rates, with
94 bottom-up studies generally finding smaller emission rates than their top-down counterparts (Brandt et al., 2014). The
95 discrepancy between the results from these two methodologies must be better understood if the true emission rate is to be
96 known. Both the bottom-up and top-down approaches have their own inherent sources of error. For the bottom-up approach,
97 a small sample size could result in the omission of any super-emitters, resulting in a low emissions bias. For the top-down
98 approach, difficulty in attributing the measured enhancements to their correct sources can lead to errors when solving for the
99 emissions of a particular sector.

100 Top-down emission estimates of individual basins have shown variation in the emission rate across the different
101 basins. An aircraft mass balance performed over the Barnett shale in Texas found an emission rate between 1.3-1.9% of



102 production (Karion et al., 2015), yet a similar mass balance study executed over unconventional wells in Uintah County, Utah,
103 calculated an emission rate between 6.2-11.7% of production (Karion et al., 2013). Differences in regional emission rates can
104 perhaps best be illustrated by recent studies in the Marcellus region. The Marcellus shale gas play is part of the Marcellus
105 geological formation running close to the Appalachian mountain chain from West Virginia to southern New York and contains
106 an estimated 140 billion cubic feet of technically recoverable natural gas (EIA, 2012). Reaching peak production by the end
107 of 2015, the Marcellus is the largest producing shale in the U.S., producing 17,000 million standard cubic feet (MMSCFD)
108 per day of natural gas (EIA, 2016a). A bottom-up study measuring emissions from 17 unconventional well-sites in the
109 Marcellus found a median emission rate from the wells of 0.13% of production, but estimated a mean emission rate of 0.53%
110 of production due to the potential presence of super-emitters which would skew the mean emission rate towards values higher
111 than the median (Omara et al., 2016). An aircraft mass balance study over northeastern Pennsylvania calculated an emission
112 rate of 0.30%, a number that accounted for emissions from the production, processing, and transmission of the gas (Peischl et
113 al., 2015). Both of these derived estimates fall below emission rates calculated throughout other basins and are below the 3%
114 threshold required for natural gas to be a smaller climate pollutant in comparison to coal over a 20-year timescale. The low
115 rates in the Marcellus compared to other regions could be the result of systematic difference within the Marcellus that leads to
116 a more efficient extraction of natural gas. However, while useful as a first-guess estimation, current studies performed in the
117 region are based on relatively small sample sizes (1 aircraft mass balance and 88 individual well measurements). A more
118 thorough analysis of the emission rate in the Marcellus would provide insight into regional differences in CH₄ emissions from
119 different shale basins and help improve national estimates of emissions from natural gas.

120 This study seeks to provide confidence in the emission rate for the northeastern Marcellus by performing the most
121 thorough top-down analysis of the northeastern Marcellus region to date. CH₄ measurements were taken from aircraft
122 observations across 10 flights in northeastern Pennsylvania. A new implementation of modelling CH₄ mole fractions is
123 developed to track complex plume structures associated with different emitters, and an optimal natural gas emission rate is
124 solved for each of the 10 flights. An aircraft mass balance technique is also conducted for 4 of the flights and natural gas
125 emission estimates from this method are compared to those calculated using the modelling technique. Using information on
126 the uncertainty with both methods, a regional emission rate is calculated for the natural gas industry in the northeastern
127 Marcellus region.

128 2 Methods

129 The objective of this study is to quantify CH₄ emissions coming from unconventional wells and compressor stations, henceforth
130 referred to as upstream natural gas emissions, in the northeastern Marcellus region (defined as the area contain within 41.1-
131 42.2°N 75.2-77.6°W, Figure 1) through two different top-down methodologies. CH₄ observations from aircraft data are
132 collected for ten (10) individual flights over a three-week period in May 2015. These data are used to solve for the upstream
133 natural gas emission rate using an aircraft mass balance approach. Additionally, a CH₄ emissions inventory for the region is



134 compiled and input into an atmospheric transport model described below. CH₄ concentrations are modelled for each flight,
135 and the upstream natural gas emission rate within the model is optimized to create the best match between aircraft observations
136 and model projected enhancement, providing another estimate for the upstream natural gas emission rate. The sections below
137 detail the regional CH₄ inventory, the aircraft campaign, the transport model, the model optimization technique, and the mass
138 balance approach used in this study.
139

140 **2.1 Regional Methane Emission Inventory**

141 In this study we characterize emissions from the natural gas industry into five different sectors: emissions from wells, emissions
142 from compressor facilities, emissions from storage facilities, emissions from pipelines, and emissions in the distribution sector.

143 To estimate CH₄ emissions from the production sector of the natural gas industry, data were first obtained on the
144 location and production rate of each unconventional well from the Pennsylvania Department of Environmental Protection Oil
145 and Gas Reporting website (PADEP, 2016) and the West Virginia Department of Environmental Protection (WVDEP, 2016).
146 To convert the production rate into an emission rate, we need to assume a first-guess as to the expected leakage from wells in
147 the area. A first-guess natural gas emission rate of 0.13% was applied to the production value of each of the 7000+ producing
148 unconventional wells based on the median rate from Omara et al., (2016). The natural gas emission rate was then converted to
149 a CH₄ emission rate by assuming a CH₄ composition in the natural gas of 95% (Peischl et al., 2015).

150 In addition to unconventional wells, the domain also contains more than 100,000 shallow conventional wells. Annual
151 conventional production rates for the year 2014 were obtained through the PADEP Oil and Gas Reporting website, the
152 WVDEP, and the New York Department of Environmental Conservation (NYDEC, 2016). Despite the large number of wells,
153 the average conventional well in PA produces 1% of the natural gas compared to its unconventional counterpart. However, it
154 is speculated that the older age of these wells and a lack of maintenance and care for them results in a higher emission rate for
155 these wells as a function of their production (Omara et al., 2016). A first-guess natural gas emission rate of 11% was applied
156 to the production values of the conventional wells based on the median emission rate from the wells sampled in Omara et al.,
157 (2016). Similar to the unconventional wells, the natural gas emission rate was then converted to a CH₄ emission rate by
158 assuming a CH₄ composition in the natural gas of 95%.

159 Compressor stations located within the basin are responsible for collecting natural gas from multiple well locations,
160 removing non-CH₄ hydrocarbons and other liquids from the flow, and regulating pressure to keep gas flowing along gathering
161 and transmission pipelines, and can be a potential source for methane emissions. Data for compressor station locations and
162 emissions comes from a dataset used in Marchese et al., (2015). A total of 489 compressor facilities are listed for Pennsylvania,
163 with 87% of the listed facilities also containing location data. Emissions for each compressor station are calculated through
164 two different methodologies. In the simplest case, a flat emission rate of 32.35 kg hr⁻¹ is applied for each station, the mean
165 emission rate of a gathering facility in PA found in Marchese et al., (2015). In the more complex scenario, the same emissions
166 total is used as in the flat rate case, but is distributed among the compressor stations linearly as a function of their energy usage.



167 Wattage between compressors in our dataset can vary greatly, from 10 kW for small compressors to 7000 kW or more at large
168 gathering facilities. Using the wattage as a proxy for emissions allows us to account for the size and throughput of natural gas
169 at each station and assumes larger stations will emit more natural gas compared to smaller stations (Marchese et al., 2015).

170 Data on locations of underground storage facilities were obtained from the United States Energy Information
171 Administration (EIA, 2015). For each of these locations, a base emission rate of 96.7 kg hr^{-1} was applied according to the
172 average value emitted by a compressor station associated with an underground storage facility (Zimmerle et al., 2016).

173 To calculate pipeline emissions, data on pipeline locations needed to be collected. Information on transmission
174 pipelines, which connect gathering compressors to distribution networks, is provided by the Natural Gas Pipelines GIS product
175 purchased from Platts, a private organization which collects and creates various infrastructural layers for the natural gas and
176 oil industry (Platts, 2016). Gathering pipeline data, corresponding to the transfer of gas from wellheads to gathering
177 compressors, is nearly non-existent for PA with the exception of Bradford County, which maps out all gathering pipeline
178 infrastructure within the county border. In PA, information on the location of a gathering pipeline elsewhere is only available
179 where a gathering line crosses a stream or river. To account for gathering pipelines in the remainder of the state, a GIS model
180 was created using Bradford County as a typical pattern to simulate connecting pipelines between unconventional wells
181 throughout the state (Figure 2). The resulting pattern follows the valley of the Appalachian Mountains, with larger pipelines
182 crossing through the state to connect the different branches of the network. These pipelines were then multiplied by an emission
183 factor of $0.043 \text{ kg per mile of pipe}$, the factor used for gathering pipeline leaks in the Inventory of U.S. Greenhouse Gas
184 Emissions and Sinks: 1990-2013 (EPA, 2015b).

185 CH_4 emissions from natural gas distribution sources, coal mines, and animal/animal waste were provided from
186 Maasackers et al., (2016), which takes national scale emissions from the EPA's greenhouse gas inventory for the year 2012
187 and transforms it into a $0.1^\circ \times 0.1^\circ$ emissions map for the continental U.S. For natural gas distribution emissions, various
188 pipeline data was collected at a state-level and emission factors were accounted for to calculate a total distribution emission
189 for the state. This emissions total was then distributed within the state proportional to the population density. Emission
190 estimates for coal are calculated using information from the Greenhouse Gas Reporting Program (GHGRP) for active mines
191 and the Abandoned Coal Mine Methane Opportunities Database for abandoned mines (EPA, 2008). State-level emissions
192 missions from enteric fermentation and manure management are provided in the EPA's inventory. These emissions were
193 segregated into higher resolutions using county-level data from the 2012 U.S. Census of Agriculture (USDA, 2012) and land-
194 type mapping.

195 Finally, the EPA's Greenhouse Gas Reporting Program dataset for the year 2014 was used to capture all other major
196 sources of CH_4 in the region otherwise unaccounted for, the majority of which are emissions from landfills and some industrial
197 sources (EPA, 2015a). Sources within the GHGRP that overlap with natural gas sources already accounted for within our
198 inventory were removed to prevent redundancy.

199 Although our emissions map used for the model runs did not account for potential CH_4 emissions from wetland
200 sources, a series of wetlands emission scenarios was obtained for the region using data from Bloom, et al., (in review). From



201 this dataset, wetland CH₄ emissions make up only 1% of all regional CH₄ emissions in the most extreme scenario, and thus we
202 assume their impact is negligible to this study.

203 2.2 Aircraft Campaign

204 Observations for this project were obtained from a 3-week aircraft campaign during the period of May 14th-June 3rd, 2015.
205 The campaign was led by the Global Monitoring Division (GMD) of the National Oceanic and Atmospheric Administration
206 Earth Systems Research and Laboratory (NOAA ESRL), in collaboration with the University of Michigan. During this period,
207 the NOAA Twin Otter aircraft flew throughout the northeast portion of Pennsylvania, providing a total of ten flights across
208 nine days. The aircraft was equipped with a Cavity Ring-Down Spectroscopic analyser (Picarro G2401-m) measuring CH₄,
209 CO₂, CO, and water vapour mole fractions at approximately 0.5Hz with a random error of 1 ppb, 0.1 ppm, 4 ppb, and 50 ppm
210 respectively (Karion et al., 2013). GPS location, horizontal winds, temperature, humidity, and pressure were also recorded at
211 1Hz. The majority of observations for each flight occurred during the afternoon hours at heights generally lower than 1000 m
212 above ground level. Each flight contains at least one vertical profile within and above the boundary layer, with temperature
213 and water vapour observations from these profiles used to estimate the atmospheric boundary layer height and ensure that the
214 aircraft sampled air within the boundary layer throughout the flight. Observations taken above the boundary layer top are
215 flagged and removed from calculation.

216 Flight paths, wind speeds, and CH₄ observations for each of the 10 flights can be seen in Figure 3. For six of the ten
217 flights, a box pattern was flown around a large portion of unconventional natural gas wells in northeastern PA. These flights
218 were performed typically on days with a strong, steady wind, with a clearly defined upwind and downwind transect intended
219 for use in an aircraft mass balance calculation. Five of the six box-pattern flights were composed of two loops circling the gas
220 basin, allowing for two separate calculations of the upstream natural gas emission rate for the flight. On the remaining four
221 flights, raster patterns were performed to help identify spatial complexities of CH₄ emissions within the basin. All ten flights
222 were used in the model optimization calculation of the upstream natural gas emission rate.

223 2.3 Transport Model

224 The atmospheric transport model used in this study is the Advanced Weather Research and Forecasting (WRF) model (WRF-
225 ARW, Skamarock et al., 2008) version 3.6.1. The WRF configuration for the model physics used in this research includes the
226 use of: 1) the double-moment scheme (Thompson et al., 2004) for cloud microphysical processes, 2) the Kain-Fritsch scheme
227 (Kain and Fritsch 1990, Kain 2004) for cumulus parameterization on the 9-km grid, 3) the Rapid Radiative Transfer Method
228 for general circulation models (GCMs) (RRTMG, Mlawer et al., 1997, Iacono et al., 2008), 4) the level 2.5 TKE-predicting
229 MYNN planetary boundary layer (PBL) scheme (Nakanishi and Niino 2006), and 5) the Noah 4-layer land-surface model
230 (LSM) that predicts soil temperature and moisture (Chen and Dudhia 2001, Tewari et al., 2004) in addition to sensible and
231 latent heat fluxes between the land surface and atmosphere.



232 The WRF modelling system used for this study also has four-dimensional data assimilation (FDDA) capabilities to
233 allow meteorological observations to be assimilated into the model (Deng et al., 2009). With WRF FDDA, observations are
234 assimilated through the entire simulation to ensure the optimal model solutions that combine both observation and the dynamic
235 solution, a technique referred to as dynamic analysis. Data assimilation can be accomplished by nudging the model solutions
236 toward gridded analyses based on observations (analysis nudging), or directly toward the individual observations (observation
237 nudging), with a multiscale grid-nesting assimilation framework typically using a combination of these two approaches (Deng
238 et al., 2009; Rogers et al., 2013).

239 The WRF model grid configuration used in this research contains two grids: 9- and 3-km (Figure 4), each with a mesh
240 of 202x202 grid points. The 9-km grid contains the mid-Atlantic region, the entire northeastern United States east of Indiana,
241 parts of Canada, and a large area of the northern Atlantic Ocean. The 3-km grid contains the entire state of Pennsylvania and
242 most of the state of New York. Fifty vertical terrain-following model layers are used, with the centre point of the lowest model
243 layer located at ~10 m above ground level. The thickness of the layers stays nearly constant with height within the lowest 1
244 kilometre, with 26 model layers below 850 hPa (~1550 m AGL). One-way nesting is used so that information from the coarse
245 domain translates to the fine domain but no information from the fine domain translates to the coarse domain.

246 FDDA (Deng et al., 2009) was used in this research, with the same strategy as used in Rogers et al., (2013). Both
247 analysis nudging and observation nudging were applied on the 9-km grid, and only observation nudging was applied on the 3-
248 km grid. In addition to assimilating observations and using the North America Regional Reanalysis model as initial conditions,
249 we reinitialize the WRF model every five days, allowing 12 hours of overlapping period in consideration of model spin-up
250 period to prevent model errors from growing over long periods. The observation data types assimilated include standard WMO
251 surface and upper-air observations distributed by the National Weather Service (NWS), available hourly for surface and 12-
252 hourly for upper air, and the Aircraft Communications Addressing and Reporting System (ACARS) commercial aircraft
253 observations, available anywhere in space and time with low-level observations near the major airports.

254 The WRF model used in this study enables the chemical transport option within the model allowing for the projection
255 of CH₄ concentrations throughout the domain. Surface CH₄ emissions used as input for the model come from our CH₄
256 emissions inventory and are all contained within the 3-km nested grid. Each source of CH₄ within our inventory is defined
257 with its own tracer (Table 1), allowing for the tracking of each individual source's contribution to the overall projected CH₄
258 enhancement within the model. For this study, CH₄ is treated as an inert gas. The potential for interaction with the hydroxyl
259 radical (OH), the main sink of CH₄, is neglected. A calculation assuming an above-average OH mole fraction over a rural
260 region of 0.5pptv (Stone et al., 2012) and a reaction rate of 6.5×10^{-15} (Overend et al., 1975) produces a CH₄ sink of 0.5ppb per
261 hour. The duration of a flight can be up to 3 hours, leading to a potential loss of 1.5ppb over the course of a flight. This loss is
262 small but not insignificant. CH₄ plumes associated with natural gas during each flight ranged between 15-70 ppb, and a change
263 of 1.5ppb could theoretically impact observations by as much as 10% of the plume signal. However, this decrease in the CH₄
264 mole fraction would likely have equal impacts on both the background CH₄ values as well as the enhancement. Because
265 emission calculations are based on the relative difference between the CH₄ background mole fraction and the enhancement



266 downwind, it would take a gradient in the oxidation of OH to impact the results. Considering this relatively low destruction
267 rate, the expected homogeneity of the sink across the region, and the difficulties associated with the simulation of chemical
268 loss processes, we assumed that the CH₄ mass is conserved throughout the afternoon and therefore we ignored the impact of
269 oxidation by OH.

270 2.4 Model Optimization Technique

271 The objective of the model optimization technique is to solve for a natural gas emission rate as a percent of natural gas
272 production that creates the best match between modelled CH₄ concentration maps, provided by the transport model, with actual
273 CH₄ mole fraction observations, provided by the aircraft data. The optimization process in this study was originally designed
274 to solve for natural gas emission from unconventional wells and emissions from compressor facilities separately. Because the
275 flow rate of natural gas being processed was not available for each compressor station, emissions at each facility were originally
276 scaled based on the size of the station. However, when running the transport model using this emissions map, enhancements
277 from the compressor stations produced plume structures nearly identical in shape to enhancements from the unconventional
278 wells due to the similar spatial distributions of these two tracers. Without distinct differences between the enhancement patterns
279 from each tracer, it becomes impossible to distinguish which emissions source must be adjusted to obtain the closest match to
280 the observations. For this reason, emissions from compressor facilities are merged with unconventional well emissions in the
281 optimized emission rate. Though the emission rate solved for in this experiment only uses the locations and production for the
282 unconventional wells, this optimized rate represents emissions from both the wells and compressor facilities and will be
283 referred to as the modelled upstream natural gas emission rate. Midstream and downstream natural gas processes (such as
284 processing, transmission and distribution of the gas) and emissions from conventional wells are not solved for in this study
285 due to their minimal contribution (less than 5%) to CH₄ emissions in the region encompassed by the aircraft campaign.

286 Using the transport model WRF-Chem, CH₄ atmospheric enhancements were generated for each flight using different
287 tracers to track different components to the overall CH₄ enhancement (e.g. animal/animal waste, distribution sector, industries).
288 From these concentration fields, the upstream natural gas emission rate was solved for each flight using a three-step model
289 optimization technique. First, a background concentration was determined for each flight and subtracted from the observations
290 to create a set of “observed CH₄ enhancements,” using

$$291 X_{EnhO} = X_{Obs} - X_{bg} \quad , \quad (1)$$

292 where X_{Obs} is the CH₄ mole fraction observation from the aircraft, X_{bg} is a chosen background value for the flight, and X_{EnhO}
293 is the calculated CH₄ enhancement at each observation. In this study, the background value is defined as the ambient CH₄ mole
294 fraction over the region not accounted for by any of the sources within the model, with each flight having a unique background
295 value. Box-pattern flights containing 2 loops around the basin may have a different background value assigned for each loop.
296 To determine the background mole fraction, we start with the value of the observed mole fraction in the lowest 2nd percentile
297 of all observations within the boundary layer for a given flight or loop. This chosen background value represents the CH₄ mole



298 fraction across the flight path from sources that are outside of our model domain. Because the background value is meant to
299 represent the CH₄ mole fraction outside the model domain which is otherwise unaccounted for in our model, using the
300 observations with the lowest CH₄ mole fraction is not always a sufficient definition for the background. On certain days, CH₄
301 enhancements from sources within the model domain can form plumes with wide spatial coverage that cover all observations
302 during a flight. For example, during a flight the lowest CH₄ observations from the aircraft may be 1850 ppb, but the model
303 simulation during that period indicates that all observations within the flight are being impacted by at minimum a 20 ppb
304 enhancement. In this case, we would set our background value for the flight at 1830 ppb, and say that our 1850 ppb observations
305 from the flight are a combination of an 1830 ppb background in addition to a 20 ppb enhancement from sources within the
306 model. By subtracting off this background value from our observations, we create a set of “observed CH₄ enhancements”
307 which can be directly compared to the model projected enhancements

308 The next step is to remove enhancements from this set that are not associated with emissions from upstream natural
309 gas using

$$310 X_{GasO} = X_{EnhO} - X_{OtherM}, \quad (2)$$

311 where X_{OtherM} is the modelled CH₄ enhancement at each observation from sources unrelated to upstream natural gas processes,
312 and X_{GasO} is the observed CH₄ enhancement associated with upstream natural gas emissions for each observation. In this step,
313 each observed CH₄ enhancement has subtracted from it the projected non-natural gas enhancement from the model (i.e. nearest
314 grid point in space) using the corresponding model output time closest to the observation within a 20-minute time interval.
315 This creates a set of observed CH₄ enhancements related only to emissions from upstream gas processes, filtering out potential
316 signals from other CH₄ emitters and providing a set of observed enhancements that can be directly compared to the projected
317 upstream natural gas enhancement within the model. By subtracting these other sources from the observations, we make the
318 assumption that our emissions inventory is accurate for non-natural gas sources and that the transport of these emissions is
319 perfect, both of which are actually uncertain. Because errors exist in both the emissions and transport, it is possible to derive
320 a negative observed upstream gas enhancement if model-projected enhancements from other sources are larger than the
321 observed enhancement. To avoid such situation, these negative observed upstream gas enhancements are set to 0. Errors
322 associated with this issue and other uncertainties with our inventory are examined further in the results section of this paper.

323 In the final step, the upstream natural gas emission rate within the model is adjusted to create the best match between
324 the modelled upstream gas enhancement and observed upstream gas enhancement using

$$325 J = \sum_{i=1}^n (X_i^{GasO} - C * X_i^{GasM}) \quad (3)$$

326 where n is the number of observations in the flight, and X_i^{GasO} and X_i^{GasM} are the observed and modelled enhancement for
327 each observation i . In this equation, J is a cost function we are trying to minimize by solving for a scalar multiplier C which,
328 when applied to the modelled natural gas enhancements, creates the smallest sum of the differences between the observed
329 upstream gas enhancement and the modelled upstream enhancement. Because the emission rate within the model is linearly



330 proportional to the model enhancements, we can solve for the upstream natural gas emission rate that minimizes the cost
331 function using

$$332 \quad E = 0.13 C \quad (4)$$

333 where 0.13 was the first guess upstream emission rate (in percent of production) used in the model, and E is the optimized
334 emission rate for the flight as a percentage of the natural gas production at each well. This final value represents an overall
335 emission rate associated with both unconventional wells and compressor stations across the region.

336 2.5 Aircraft Mass Balance

337 An aircraft mass balance calculation was performed for four applicable flights from the aircraft campaign as an alternative
338 method to calculate upstream natural gas emission rates independent of the transport model. The aircraft mass balance approach
339 uses the CH_4 enhancement between a downwind and upwind transect to calculate the total CH_4 flux of the area contained
340 between the two transects. We use the mass balance equation from Karion et al., (2013):

$$341 \quad E = \bar{U} \cos(\bar{\theta}) \int_{-b}^b \Delta X \int_{z=0}^{z_{top}} n_{air} dz dx \quad (5)$$

342 where E is the total flux (in mol s^{-1}) coming from the enclosed flight track, \bar{U} is the mean wind speed (in m s^{-1}), $\bar{\theta}$ is the mean
343 angle of the wind perpendicular to the flight track, ΔX is the CH_4 enhancement measured along the downwind flight track from
344 $-b$ to b (expressed as a mole fraction), n_{air} is the molar density of air within the boundary layer (in mol m^{-3}), and each of the
345 integrals represents the summing over all air being measured within our transect in both the horizontal (x) and the vertical (z).
346 By simplifying further and using the mean enhancement along each downwind transect as the enhancement and choosing z_{top}
347 to be the top of the boundary layer, we can transform the previous equation into the following:

$$348 \quad E = 37.3(L)(D)(\bar{U})\Delta\bar{X}\cos(\bar{\theta}) \quad (6)$$

349 where L is the length of the transect (in meters), D is the depth of the boundary layer (in meters) found using observations
350 from vertical ascents during each flight, $\Delta\bar{X}$ is the mean enhancement across the transect (expressed as a mole fraction), \bar{U} and
351 $\bar{\theta}$ are the mean wind speed (in m s^{-1}) and wind direction relative to the angle of the transect, and 37.3 is the average molar
352 density of dry air within the boundary layer (in mol m^{-3}) assuming an average temperature and pressure of 290K and 900hPa.

353 Flights on May 22nd, May 23rd, May 28th, and May 29th, 2015 were selected for mass balance calculations based on
354 their box-shaped flight patterns surrounding a large portion of the northeastern Marcellus gas basin, reasonable steady-state
355 wind conditions during the flight (this eliminated May 14th when a low pressure system was stationed over the region), and a
356 lack of strong CH_4 enhancements originating from outside of the box which could affect both the upwind and downwind
357 transects. Emission rates within the enclosed region were calculated from each of these flights, and emissions not associated
358 with unconventional gas production and gathering sources within the box were subtracted out using information from our
359 inventory. A ratio was taken of the calculated emission rate to the total production in the box, and an upstream natural gas



360 emission rate based on production was obtained. For each of the May 22nd, May 23rd, and May 28th flights, two loops of
361 similar structure and at similar altitudes were performed around the basin, allowing for two individual mass balance
362 calculations on these days. An emission rate is calculated for each of these loops and the two values are averaged to calculate
363 the daily emission rate.

364 **3 Results**

365 **3.1 Methane Inventory**

366 From the CH₄ inventory created in this study, a total anthropogenic CH₄ emission rate of 2.76 Tg CH₄ year⁻¹ is projected within
367 our inner model domain (Figure 5) with values for individual source contributions shown in Table 2. This total emissions
368 estimate assumes a leak rate of 0.13% of gas production for unconventional wells, and does not account for emissions from
369 natural gas transmission and storage facilities outside of PA due to a lack of information available from other states. Within
370 the model domain, the area encompassing southwestern PA and northeastern WV stands out as the largest contributor to CH₄
371 emissions, with emissions from conventional gas, unconventional gas, and coal mines all having significant contributions to
372 the total. In particular, the large emissions from coal make this region unique in comparison to other shales. The EPA's
373 Greenhouse Gas Reporting Program dataset for the year 2014 lists individual coal mines in the southwestern portion of our
374 domain as 8 of the top 10 CH₄ emitting facilities across the entire United States. This large area source of CH₄ can have an
375 impact on CH₄ concentrations hundreds of kilometres downwind and must be taken into account when winds are from the
376 southwest (Figure 6). Examples of this plume and its impacts on the aircraft campaign are discussed in Section 3.2.1.

377

378 **3.2 Model Optimization Results**

379 **3.2.1 Case Studies**

380 From the aircraft campaign, a total of 10 flights across 9 days were used in the model optimization technique. For each one of
381 these flights, CH₄ concentration fields were produced using WRF-Chem, and the emission rate from upstream gas processes
382 was adjusted as outlined in the methods section to find the rate that best matches the total observed CH₄ enhancement. For box
383 flights with two loops completed around the basin, emission rates were calculated for each loop independent from one another
384 and then averaged for the flight. Table 3 provides the general meteorology for the 10 flights.

385 During each of the observational periods, we use the transport model to project the mole fraction enhancement across
386 the region for each of the different CH₄ tracers (Figure 7). From these projections, we see three common sources of CH₄ which
387 can significantly influence the observed mole fractions in our study region of northeastern PA. The first is emissions from
388 unconventional gas in northeastern PA. Although the first-guess total emissions from upstream production in the Marcellus
389 are small compared to the overall contributions from other sources within the domain, their proximity to the aircraft track



390 results in unconventional gas having the largest contribution to observed enhancements throughout the domain covered by
391 most of the flights, often producing signals downwind of about 20-80 ppb above background levels. The second most
392 influential source of enhancements in our study region comes from various sources of CH₄ emissions located in southwestern
393 PA. Despite being more than 400 km away from our study region, large plumes from coal and other sources in the southwestern
394 corner of the state can contribute enhancements as high as 50 ppb across portions of the flight when winds are from the
395 southwest, affecting background measurements and masking signals from the unconventional gas. One final, but less
396 influential source of CH₄ enhancement is animal agriculture in southeastern PA. Lancaster County is home to roughly 20% of
397 all cattle in the state, with more than 200,000 cattle and calves as of 2012. A southerly wind can result in a 5-15 ppb
398 enhancement across the flight path due to enteric fermentation and manure management from these cattle. Because of coal,
399 conventional gas, and cattle sources located south of the basin, signals from flights with a southerly component to the wind
400 can be difficult to interpret without modelling the projected plumes associated with these sources. Observations on these days
401 contrast to days with a northerly wind component, where a lack of CH₄ sources north of the study region results in observations
402 with a more clearly defined background and unconventional natural gas enhancement.

403 For each of the ten flights, variability in the model-observation offset was observed. The first loop of the May 29th
404 flight is the best example of a case where comparisons between the modelled and observed enhancements match closely after
405 optimization. For this flight, a box pattern was flown encompassing a majority of the unconventional wells in northeastern PA,
406 and enhancements were observed along the western and northern transects of the flight. Modelled enhancements from sources
407 unrelated to upstream gas emissions showed a broad CH₄ plume associated mostly with animal agriculture along the western
408 edge of the flight, and a smaller enhancement on the eastern edge associated with two landfills in the Scranton/Wilkes-Barre
409 urban corridor (Figure 8). Both of these enhancements are subtracted off from the observations to produce a set of observed
410 enhancements due to natural gas production and gathering facilities. Any enhancements in this new observational dataset are
411 located almost entirely along the northern transect of the flight, directly downwind of the natural gas activity in the region.
412 The observed upstream gas enhancement is then directly compared to the modelled upstream enhancement using its first guess
413 emission rate, and an optimized upstream emission rate of 0.26% of production (i.e. a doubling of the first guess) is calculated
414 by minimizing the difference between the two datasets (Figure 9).

415 The match between observed and modelled CH₄ enhancements on the first loop of the May 29th flight is closer than
416 any other flight in the campaign, with a correlation coefficient of 0.73. The success of the model on this day is likely due to a
417 number of ideal conditions. In general, inconsistencies between the modelled and observed mean wind speeds and boundary
418 layer heights can have a linear bias on the projected enhancements, but for this flight differences between the observed and
419 modelled wind speed and boundary layer height were near 0 for both loops (Figure 10, 11). Observed wind directions
420 throughout the course of the flight had little spread, resulting in a transport of the CH₄ plumes that the model was able to match
421 well. Furthermore, the observed mean wind speed was 4.6 m s⁻¹, a moderate wind which allows for a steady transport of any
422 enhancements towards the downwind transect, but not strong enough to dilute their magnitude, resulting in an easily observable
423 enhancement downwind of the basin. Finally, intrusions from sources unrelated to upstream gas were small on this day due to



424 favourable wind conditions, reducing the probability of incorrectly attributing the observed enhancements to the wrong source.
425 Enhancements from upstream natural gas processes were around 30 ppb along our downwind transect. By comparison,
426 enhancements from other sources were lower than 15 ppb along a majority of the flight, and most of these enhancements were
427 located west of the downwind transect, making them easier to identify and remove without unintentionally impacting
428 enhancements from the natural gas plume. All of these different factors likely contributed to producing a situation where the
429 model was successfully able to match CH₄ observations during the May 29th flight.

430 Flights that occurred on days with a southwest wind had a tendency to produce CH₄ observations that were intuitively
431 difficult to interpret due to convolved CH₄ sources in southwestern Pennsylvania. One of these complex observation sets
432 occurred during the late afternoon flight on May 24th, 2015 (Figure 12). Observations on this day show a CH₄ enhancement
433 pattern that decreased with latitude, with higher CH₄ mole fractions observed farther south. Given the location of the wells in
434 the middle of the flight path and the WSW wind pattern in the region, this north/south CH₄ gradient is unexpected and
435 counterintuitive compared to where one would expect the enhancements to be based solely on the presence of the gas industry
436 in northeastern PA. However, through modelling each of the many contributors of CH₄ within our inventory, we are able to
437 recreate this latitudinal CH₄ gradient and better understand the observed patterns (Figure 12). Throughout an 18-hour period
438 leading up to the May 24th flight, winds from the SSW transport emissions from coal in southwestern PA northeastward until
439 they reach the centre of the state, where a westerly wind then shifts the plume across the study region such that it only intersects
440 the southern half of the flight path. Because of both the magnitude of the coal emissions and an accumulation that occurred in
441 the southwestern portion of the state during the previous night, the modelled enhancement from the coal plume is substantial
442 (>20 ppb) as it crosses over the flight path and covers up much of the signal from upstream gas emissions. Nonetheless, the
443 transport model is able to account for these far-reaching sources and separate out their contribution to the observed
444 enhancements. We are able to solve for the optimal upstream natural gas emission rate and recreate the May 24th flight
445 observations more accurately than most other flights, with a correlation coefficient of 0.71 between the observations and model
446 values.

447 Despite the model's success at recreating observations from the May 24th late-afternoon flight, there is reason to be
448 careful when interpreting results from observations influenced by distant sources. In particular, some transport error is
449 unavoidable in atmospheric reanalyses, and the longer the time and distance a plume takes to reach the observations, the more
450 its position and magnitude will be susceptible to these errors. During the early May 24th flight, a small 50 km shift in the
451 location of the coal plume across the study region would change projected enhancements at some observations by as much as
452 20 ppb. Furthermore, errors in the transport speed could create scenarios where the coal plume either arrives in the study region
453 too early or exits too late, creating a projected enhancement pattern that does not agree with the observations (Figure 13).
454 Additionally, inaccuracies with the emission estimates of non-unconventional gas sources in the inventory will impact the
455 magnitude of their CH₄ enhancements, creating additional errors in the optimization process when subtracting out these
456 enhancements from the observations. The early-afternoon May 24th flight and May 25th flight are both examples where
457 influences from CH₄ sources in southwest PA create complex structures in the enhancements, which the model is not able to



458 match as well as the late-afternoon flight on May 24th (Figure 14). And although observations and modelled enhancements
459 closely match throughout portions of these two flights, a slight shift in the modelled wind direction can lead to vastly differing
460 results due to the large offset small changes in the wind field can have on an emission source hundreds of kilometres away.
461 Thus, results from the flights on May 24th and May 25th should be taken with caution. A deeper analysis of these errors can be
462 found in Section 3.2.2.

463 Though transport errors from far off sources can have significant impacts on the optimized emission rate, more local
464 transport error is handled more effectively in the model through use of the error minimization cost function discussed in the
465 methods section (Eq. 3). Through use of this cost function, we solve for an upstream emission rate that minimizes the area
466 under the curve between the observed and modelled enhancement. This analysis produces a compensation effect that can adjust
467 for misalignment between the observed natural gas CH₄ plume and the modelled plume, and works best for local sources
468 whose plume structure is similar between the model and observations but location is misaligned. The impact of this effect can
469 be seen best for the flight of May 14th, 2015 (Figure 15). During this day, high pressure was centred just north of the flight
470 track, creating diverging winds that were difficult for the transport model to simulate, and the major plume associated with
471 upstream gas emissions ends up south of a well-defined plume in the observations. Despite this misalignment, the model still
472 simulates the correct magnitude and width of the plume, providing confidence that small errors in the transport of local, well-
473 defined structures have only a small impact on the overall emission rate calculation for any given flight. This assumption is
474 corroborated by an analysis of simulated enhancements of an aircraft transecting a plume at an angle of 45° with errors in the
475 projected wind direction varying between ±20°. Such angle would produce errors in the optimized emission rate ranging from
476 ±30% (Figure 16). These errors become smaller as the angle of the aircraft's path with the axis of the major plume approach
477 90°. Because the downwind transect of most flights is often close to perpendicular with the plume from upstream gas sources,
478 and differences between modelled and observed winds are often less than 20°, emission estimate errors associated with
479 incorrect transport of the CH₄ plumes would be less than 30%.

480 3.2.2 Emission Rates and Uncertainty Assessment

481 For each of the ten flights, an uncertainty assessment was performed to obtain a range of likely upstream emission rates for
482 any individual flight. Five different sources of error were considered in this assessment: model wind speed error, model
483 boundary layer height error, CH₄ background error, CH₄ emission inventory error, and model/observation mismatch error.
484 These five sources of error vary substantially from flight to flight depending on conditions, and each can have significant
485 impacts on the total uncertainty.

486 Errors in the modelled wind direction and boundary layer height have impacts on our emission estimates which have
487 a linear impact on the results. If we assume a constant wind speed, a constant boundary layer height, and no entrainment of air
488 from the top of the boundary layer, we use the following equation to understand these impacts.

$$489 \Delta C = \overline{F}_0 \left(\frac{\Delta x}{U * D} \right) \quad (5)$$



490 where ΔC is the total CH_4 enhancement of the column of air contained within the boundary layer, \bar{F}_0 is the average emission
491 rate over the path the parcel travelled, Δx is the distance the column of air travelled, U is the wind speed and D is the boundary
492 layer height. Using this equation, we can see the linear relationship between the model wind speed, model boundary layer
493 height, and the calculated emission rate. As an example, if wind speeds in the model are biased low, natural gas enhancements
494 projected by the model would increase inversely. To compensate for this effect, the optimized emission rate would decrease
495 proportionally. A similar case can be made for bias in the boundary layer height. Both errors in the wind speed and boundary
496 layer height have known impacts on the optimized emission rate which can be corrected for, so long as the errors of each are
497 known.

498 To calculate the error in the model wind speed, we assume aircraft observations are truth and use

$$499 \quad U_e = \frac{\bar{U}_m - \bar{U}_{obs}}{\bar{U}_{obs}} \quad (6)$$

500 where \bar{U}_{obs} is the mean observed wind speed by the aircraft across all points within the boundary layer, \bar{U}_m is the mean
501 modelled wind speed by the model across all points closest in time and space to each observation, and U_e is the wind speed
502 error percentage.

503 To compute the error in the modelled boundary layer height, the observed boundary layer height for each flight is
504 assumed to be the true boundary layer height and the boundary layer height percentage error, H_e , is estimated using:

$$505 \quad H_e = \frac{\bar{H}_m - \bar{H}_{obs}}{\bar{H}_{obs}} \quad (7)$$

506 where \bar{H}_{obs} is the average observed boundary layer height across each of the aircraft profiles for a given flight, \bar{H}_m is the model
507 boundary layer height closest in time and space to the location of the observed profiles averaged over all profiles. For both the
508 observation and the model, boundary layer heights were determined by locating height of the potential temperature inversion
509 associated with the top of the boundary layer (Figure 11). In cases where a potential temperature inversion could not easily be
510 identified, changes in water vapour, CO_2 and CH_4 mixing ratios were used to identify the boundary layer top.

511 Errors in the model wind speed and boundary layer height are calculated for each of the ten flights. From these errors,
512 a corrected optimized emission rate is calculated for each flight using Eq. (8):

$$513 \quad E_{new} = \frac{E}{(1+U_e)(1+H_e)} \quad (8)$$

514 where E is the original emission rate and E_{new} is the corrected optimized upstream natural gas emission rate as a percent of
515 production. Table 4 shows the wind speed and boundary layer height errors for each flight as well as the optimized and
516 corrected natural gas emission rates. On days where model performance was poor in regards to the wind speed and boundary
517 layer height, we can see changes in the corrected emission rate. For most days, this change is less than 20% different than the
518 original optimized emission rate. However, both May 14th and May 25th have corrected emission rates which are around a
519 factor of 2 different from their original value. Whether these corrected emission rates are more accurate than the original



520 optimized rates is debatable. To calculate these alternative emission rates, we must assume that the wind speeds and boundary
521 layer heights from our limited number of observations are the true values in the atmosphere, which may not be the case.
522 Regardless of which rate is more accurate for each flight, the overall 16% high bias in the model wind speed and the -12% low
523 bias in the model boundary layer result in compensating errors that cancel out, and the mean emission rates across all flights
524 end up equal. Thus, any errors associated with these two meteorological variables has a trivial impact on the overall calculated
525 emission rate for the region and the uncorrected emission rates are used for the final mean and uncertainty calculations.

526 In addition to errors related to wind speed and boundary layer height, we quantify three other sources of error in each
527 flight: errors in the selected CH₄ background value, errors in the CH₄ inventory, and errors associated with the overall model
528 performance (Table 5). Unlike the wind speed and boundary layer errors which have easily computable impacts on the emission
529 estimates, these other three sources of error and their impact on the optimized emission rate are more difficult to quantify.

530 The background error relates to the value chosen for each flight which represents the ambient CH₄ concentration in
531 the boundary layer unrelated to emission sources within the model. In this study background values ranged from 1897-
532 1923ppb. Though background values should not have high variability during a 2-3 hour mid-afternoon flight, entrainment from
533 the boundary layer top can lead to the mixing in of tropospheric air that has different CH₄ mole fraction values from those
534 within the boundary layer, resulting in a change in the afternoon background value with time. Furthermore, for days on which
535 all aircraft observations (including those upwind of the unconventional wells) are impacted by various CH₄ plumes predicted
536 within the model, it is difficult to determine the background CH₄ concentration accurately. Additionally, observations
537 corresponding to locations with no modelled enhancement may in fact have been impacted by missing sources in our inventory,
538 highlighting the difficult nature of knowing with certainty where and what the background is for any given flight.
539 Understanding this uncertainty is crucial; any error in subtracting off the background value directly impacts each observation's
540 observed natural gas enhancement. For example, a background value of 1 ppb below the true background for a given flight
541 would add 1 ppb to each observed natural gas enhancement for all observations, creating a high bias with the optimized
542 upstream emission rate. To account for this error, each flight's optimization processes was rerun iterating the background value
543 by ± 5 ppb, and the ratio of the percent change in the emission rate compared to the original case was defined as the resulting
544 error in the emission rate due to background uncertainty. This ± 5 ppb background error range is an estimate at the range of
545 possible error in the background based on changes observed in the upwind measurements from each of the flights and is meant
546 to be a conservative estimate of the error. The impact this error can have in the emission rate varies depending on the magnitude
547 of the observed downwind enhancements during a flight. A plume containing a CH₄ enhancement of 50 ppb will have a smaller
548 relative error from a 5 ppb change compared to one with an enhancement of only 10 ppb. Thus, days with high wind speeds
549 and a high boundary layer height (and thus enhancements of a smaller magnitude) tend to be affected the most by background
550 errors.

551 Similar to background errors, errors from the CH₄ emissions inventory are difficult to quantify. In the model
552 optimization technique, we subtract out enhancements from sources unrelated to unconventional natural gas before solving for
553 the upstream gas emission rate. In doing so, we are making the assumption that our emissions inventory for sources unrelated



554 to upstream natural gas processes are accurate. In truth, each emission source in our inventory comes from a different dataset
555 and has its own unique error bounds, many of which are unknown. Because of the potential for errors in these emission
556 estimates, we take a conservative approach and iterate the unconventional emissions optimization approach for each flight,
557 varying the emissions from other unsolved for emission sources in the model by a factor of 2 in each direction, thus applying
558 a range of 50-200% to the emissions inventory values to assess its impact on the calculated upstream natural gas emission rate.
559 Despite the extensive range of emissions used in the error analysis, its impact is minimal on most days due to the northeastern
560 Marcellus region having very few emission sources not related to upstream gas processes. Only for the flights on May 24th do
561 we see errors from the inventory contribute significantly to the overall daily error, when the coal plume in southwestern PA
562 enters the centre of the study region and has a large role in the upstream emission rate calculation for that day.

563 The final source of error accounted for attempts to quantify the similarity of the pattern of modelled and observed
564 natural gas enhancements, referred to here as the model performance error. Figure 17 shows an example of two days, one of
565 which the model appears to recreate the observations, and the other of which the model poorly matches the shape of the
566 observed enhancements. Comparing these two simulations with no other information, we hypothesize that one should put more
567 trust in the upstream natural gas emission rate calculated for the flight whose modelled upstream enhancements match
568 structurally compared to the emission rate from the flight whose modelled enhancement bares little semblance to the observed
569 enhancement. The model performance error is designed to account for the trustworthiness of the optimized upstream emission
570 rate based on how well the model simulates a given day. The model performance error is calculated using Eq. (9):

$$571 \quad e_{perf} = \frac{\bar{\sigma}_{\Delta X}}{\Delta X_{gas}} \quad (9)$$

572 In this equation, $\bar{\sigma}_{\Delta X}$ is the standard deviation of the difference between the modelled and observed upstream natural gas CH₄
573 enhancement using the optimized emission rate, and ΔX_{gas} is the observed magnitude of enhancement from the major natural
574 gas plume observed in each flight. Here, ΔX_{gas} serves as a normalization factor to account for the varying strength of the
575 enhancement from flight to flight, and ensures that days with increased enhancements due to meteorological conditions or true
576 daily fluctuations in the upstream natural gas emissions do not proportionally impact the performance error percentage. For
577 example, a day with high winds and a deep boundary layer would produce smaller enhancements, leading to a small $\bar{\sigma}_{\Delta X}$
578 regardless of model performance unless normalized by ΔX_{gas} .

579 Table 5 summarizes the background error, inventory error, and model performance error, and assumes independence
580 between the three error sources to calculate the total error for each flight. The largest error occurred during the May 22nd flight,
581 where an unexplained enhancement along the northern transect led to a poor match between the modelled enhancements and
582 the observed enhancements. This may explain the anomalously high optimized emission rate for that day. Other flights with
583 large error are those which occurred on May 24th and May 25th, both days where enhancements from southwestern PA are
584 believed to be influencing observations.



585 Based on the conservative methodology used to calculate these errors, we assume the total error for each flight
586 represents a 2σ range of possible emission rates and calculate a weighted mean and a 2σ confidence interval for the overall
587 upstream emission rate across the ten flights. From this approach, we find a mean upstream emission rate of 0.36% of
588 production and a 2σ confidence interval from 0.27-0.45% of production.

589 3.3 Aircraft Mass Balance Results

590 In addition to the model emission optimization, a simplified aircraft mass balance technique was used to calculate upstream
591 natural gas emission rates for flights with a box-pattern, a consistent wind direction within the box, and minimal intrusion of
592 CH₄ enhancements from outside the study region that would affect both the upwind and downwind transects. Of the 6 days
593 with box-patterned flights from the aircraft campaign, one day (May 14th) contained a surface low-pressure centre in the middle
594 of the flight resulting in erratic wind patterns, and another day (May 25th) had CH₄ plumes from southwestern PA affecting
595 portions the flight observations. These days were not used for a mass balance, and calculations were performed for the
596 remaining box-pattern flights (May 22nd, May 23rd, May 28th, May 29th). Of the four remaining flights, three of these flights
597 contained two loops around a portion of the Marcellus basin. A mass balance was performed on each loop, resulting in a total
598 of 7 mass balance calculations for the region across 4 days. Table 6 summarizes the results from the mass balance flights.

599 For each flight, a total flux within the box encompassed was calculated using Eq. (6). Using this flux, a natural gas
600 emission rate based on production from within the box was calculated using Eq. (10)

$$601 \quad E_{\%} = \frac{E - E_{other}}{P} \quad (10)$$

602 where E is the total flux from Eq. (6) (in kg hr⁻¹), E_{other} are the emissions enclosed in the box from sources not related to
603 upstream natural gas processes (in kg hr⁻¹), P is the total CH₄ from natural gas being produced within the box (in kg hr⁻¹), and
604 $E_{\%}$ is the resulting natural gas emission rate as a percent of total production within the box. Calculated emission rates varied
605 extensively between flights, ranging from 0.11% to 1.04% of natural gas production. Comparing emission rates between loops
606 on the same day, we see more consistency in the values. This result is not surprising, as on each of the days with multiple
607 loops, upwind and downwind CH₄ concentrations patterns tended to be similar between loops. Thus, differences in the total
608 emission rate are likely due to either errors specific to each day (such as background variability, errors in meteorology) or real
609 daily variability in the upstream natural gas emission rate.

610 As an error analysis for the mass balance flight, we look at four potential sources of error (Table 7). One source of
611 uncertainty comes from the observed wind speed used in Eq. (6). For our experiment, we take the mean observed wind speed
612 from the aircraft and assume this value represents the mean wind speed within the entire box during the 2-3 hour period it
613 would take for air to travel from the upwind transect to the downwind transect. To understand the uncertainty and biases
614 associated with this assumption, we recreate wind observations along the flight path using values from WRF-Chem, and
615 compare the mean wind speed from the simulated observations to the mean model winds contained within the box integrated
616 throughout the boundary layer during the 3 hour period closest to the flight time. By making this comparison, we are able to



617 understand the representation error associated with treating the wind speed observations from the aircraft as the wind speed
618 within the entire box during the period it would take for air to cross from the upwind transect to the downwind transect. On
619 average, modelled wind speeds following the flight were 7% faster than integrated wind speeds within the box, due to the
620 inability for aircraft observations to account for slower wind speeds closer to the surface. This bias was removed from each
621 day's calculated wind speed. After accounting for the wind speed bias, the average error of the modelled wind speed following
622 the flight path compared to the modelled winds within the box was 3%. This 3% uncertainty was applied to each flight and
623 used as the potential uncertainty in the mean wind speed. Errors in the wind direction were neglected, as each flight used in
624 the mass balance completely surrounded the basin using downwind transects at multiple angles, and thus small errors in the
625 wind angle would result in a negligible net change on the total flux calculated.

626 Another source of uncertainty is error in the boundary layer height. For each flight, between 2-3 vertical profiles were
627 performed, and the mean height was used in Eq. (6). The standard deviation of different heights from each transect was used
628 as the uncertainty. On May 22nd, a boundary layer height could be interpreted from only one vertical transect. For this day, we
629 assume an uncertainty of $\pm 200\text{m}$ ($\pm 9\%$).

630 Uncertainty in the CH₄ background mole fraction was estimated similarly to the boundary layer height. On three of
631 the four flights, two upwind transects were performed. The mean observed CH₄ mole fraction between the two transects was
632 used as the background value for the entire flight, and the standard deviation between the loops was used as the uncertainty.
633 On both the May 23rd and May 28th flights, background differences between the two transects were less than the instrument
634 error of 1 ppb. On these days, we use the instrument error as the background error. On May 22nd, only one upwind transect
635 was usable for the calculation. For this day, we assume a conservative estimate in the uncertainty of the background of ± 5 ppb.

636 Finally, we assess uncertainty in the emissions inventory. After a CH₄ flux is calculated for each loop, emissions from
637 sources contained within the box that are not associated with upstream natural gas processes must be subtracted out to solve
638 for the upstream natural gas emission rate. Any errors associated with our inventory will result in a CH₄ source attribution
639 error. To account for the potentially large uncertainty with the emission sources in our inventory, we vary these non-natural
640 gas emissions by a factor of 2 to test the impact on the solved upstream natural gas emission rate. Because northeastern
641 Pennsylvania contains few sources of CH₄ emissions outside of natural gas production, the impact of this uncertainty is
642 typically less than 20% of the total emissions calculated within the box.

643 From Table 7, we can see the largest relative errors occur on the May 22nd flight. It is on this day where we have the
644 largest uncertainty in the background value, with observations towards the end of the flight becoming unusable due to a rapid
645 and unexplained decrease in the CH₄ mole fraction with time (Figure 18). This day also features the highest boundary layer
646 height and fastest winds of all flights done in this study, reducing the magnitude of the enhancement associated with the natural
647 gas plume and thus amplifying the effects an uncertain background has on the overall uncertainty of the calculated CH₄ flux.
648 Uncertainty across the other three flights is smaller, and results between individual loops on the May 23rd and May 28th flight
649 provide more confidence in the calculated flux for those days.



650 Using the mean estimated CH₄ emissions and uncertainty for each loop, we calculate a daily mean emission rate and
651 uncertainty for each of the four days. We then solve for an unweighted mean across the four flights to derive our overall
652 emissions estimate from the aircraft mass balance approach, and use the standard error of the flights to estimate the uncertainty.
653 In doing so, we derive a natural gas emission rate from upstream processes of 0.34% of production, with a 2σ confidence
654 interval from 0.06-0.62% of production. Here, we use the arithmetic mean rather than a weighted mean due to the linear
655 relationship between the size of the emission rate and the size of the errors. Because errors associated with ABL height and
656 wind speed have a proportional impact on the calculated emissions within the box, days with a high emissions estimate produce
657 large uncertainties relative to days with a small emission rate. Using a weighted mean approach assigns more weight to the
658 days with low estimated emissions, and produces an overall emission estimate too low and certain to have confidence in
659 (0.12±0.02 percent of gas production).

660

661 4 Discussion

662 4.1 Upstream Emission Rate

663 From this study, we estimate with a 2σ confidence interval an emission rate between 0.27-0.45% of gas production using the
664 model optimization method and 0.06-0.62% of gas production using the aircraft mass balance. Figure 19 provides the emission
665 range estimates from upstream natural gas processes using both the model optimization technique and mass balance technique
666 when applicable. These emission rate estimates as a percent of production are the lowest observed from top-down
667 measurements of different basins in the U.S., and raise questions as to why these values in the northeastern Marcellus region
668 appear to be low. One possibility may be related to the well efficiency of the northeastern Marcellus region compared to other
669 major shale plays (Table 8). In terms of gas production per unconventional well, the Marcellus is the highest of all major basins
670 in the U.S. Furthermore, the gas production per well increases by nearly a factor of two when focusing specifically on
671 Susquehanna and Bradford Counties in northeastern Pennsylvania where the majority of the wells from this study are located
672 (Figure 20). The large difference in production per well between the northeastern Marcellus and other shales may partly explain
673 the low emission rates as a percentage of production. Throughout this study, we normalize natural gas emissions as a percentage
674 of total production under the assumption that higher throughput of natural gas in a system should lead to higher emissions in
675 the system. However, if leaks are more influenced by the number of pneumatic devices rather than the throughput passing
676 through the device, a high-efficiency system such as the northeastern Marcellus could end up having a very low emission rate
677 as a percentage of production, but a similar emission rate compared to other basins based on the number of wells, compressors,
678 etc. A thorough bottom-up study of the Marcellus region measuring emissions on a device level could provide an answer to
679 this hypothesis.



680 4.2 Advantages of Combining Observations with Model Output

681 One of the major advantages of using a chemical transport model to solve for natural gas emission rates compared to a standard
682 mass-balance approach is that the transport model is able to account for the complex and oftentimes non-uniform plume
683 structures originating from sources outside the flight path that can affect observations. When performing a mass balance over
684 a basin, it is assumed that the upwind transect is representative of the air exiting the downwind transect after subtracting out
685 all sources within the box. However, this assumption is only true if winds contained within the flight path are in perfect steady
686 state during the time it take for air to move from the upwind transect to the downwind transect, and that measurements from
687 the downwind transect occurred at a much later time so that the air being measured is the same air measured from the upwind
688 transect. These conditions are not easily achieved for regional scale mass balances due to the long times needed for the air
689 from the upwind transect to reach the downwind transect. As an example, from the four mass balance flights performed for
690 this study the average time for air to move from the upwind transect to the downwind transect was 4 hours whereas the average
691 time between the aircraft's upwind and downwind measurements was ~40 minutes. The aircraft observations can be thought
692 of as a snapshot in time, which can be problematic if large scale plumes from outside the domain are moving through the
693 region and impacting only certain portions of the observations during the flight's short timeframe. By using a transport model
694 for a domain much larger than that of the flight paths, we are able to track these far-reaching plumes and identify situations
695 where the background CH₄ concentrations may be spatially heterogeneous.

696 The potential usefulness of using a transport model alongside a mass balance calculation can best be demonstrated
697 from observations taken over the Marcellus during a 2013 aircraft campaign (Peischl et. al 2015). During this flight the
698 prevailing winds were from the WSW, and the largest CH₄ enhancements were observed along the western edge of the flight
699 path, upwind of the unconventional wells. Using our transport model, we are able to recreate the day of flight and attempt to
700 use our inventory and explain this feature (Figure 21). Comparisons between modelled output and observations show a 60 ppb
701 CH₄ enhancement from coal and conventional wells in southwest PA stretching close to the western edge of the aircraft
702 observations, a plume structure similar to the one observed during the May 24th flight from our own study. Though this plume
703 does not initially align with the observed transect with the largest enhancements, we recognize that the coal and gas plume
704 travels for more than 20 hours (a distance of 400 km) from its source before reaching the flight path. If we allow for a 10%
705 error in the transport speed and therefore advance the transport model by an additional two hours past the time in which the
706 aircraft observed these high values, we are able to line up the centre of the plume with the largest observed CH₄ mole fractions
707 along the western edge of the flight. In addition to the 60 ppb enhancement along the centre of the plume, the model projects
708 20 ppb enhancements along the edges and in front of the plume centre. These smaller enhancements have an influence along
709 different portions of the flight which varies in magnitude, making it difficult to assess a proper background CH₄ value upwind
710 of the wells and potentially masking natural gas enhancements downwind of them. But by using a transport model, we are able
711 to see the potential impact of these far-reaching sources which would otherwise not be considered in a regional mass balance
712 and better understand the complex CH₄ plume structures which can occur in a given region under specific wind conditions.



713 5 Conclusion

714 Using the model optimization technique presented in this study, we find a weighted mean natural gas emission rate from
715 unconventional production and gathering facilities of 0.36% of production with a 2σ confidence interval from 0.27-0.45% of
716 production. This emission rate is supported by four mass balance calculations, which produce a mean of 0.34% and a 2σ
717 confidence interval from of 0.06-0.62% of production. Applied to all the wells in our study region, this mean rate results in a
718 leakage rate of 20 Mg CH₄ hr⁻¹. The emission rate found in this top-down study quantified as a percent of production is
719 significantly lower than rates found using top-down methodology at any other basin, and indicates the presence of some
720 fundamental difference in the northeastern Marcellus gas industry that is resulting in more efficient extraction and processing
721 of the natural gas.

722 The ten flights that took place in this study reveal large regional variations in the CH₄ enhancement patterns depending
723 on the prevailing wind direction. On days with a northwest wind, observed enhancements come primarily from the natural gas
724 industry, and a small plume associated with it can be seen on the downwind leg of each flight with few enhancements upwind
725 of the wells. Flights which took place with winds conditions predominantly from the southwest were more difficult to
726 interpret. Plumes associated with coal and other potential sources of CH₄ in the southwestern Pennsylvania create complex
727 enhancement patterns affecting both the upwind and downwind portions of the flight, making both the background CH₄ mole
728 fraction and enhancements from the gas industry difficult to interpret. The stark difference between observations which
729 occurred with a northwest wind compared to a southwest wind illustrates the importance of having multiple flights across days
730 with various wind conditions to better understand the major influences on CH₄ concentrations throughout a region. The
731 regional influences in Pennsylvania also demonstrate the utility of deriving an emissions inventory that provides input data to
732 drive a transport model, allowing one to forecast CH₄ mole fractions on difficult days and better understand the daily
733 uncertainties associated with heterogeneous background conditions.

734 Though this study presented observations from ten flights over a three-week period, it is not able to account for the
735 potential of long term temporal variability in the emission rates. In May 2015 when the flights took place, the entire Marcellus
736 basin was nearing peak production and active drilling and hydraulic fracturing was still ongoing in the region. By mid-2016,
737 the rate of drilling of new wells in the northeast Marcellus had decreased and natural gas production had begun to decline in
738 the area. A snapshot of the emission rate during one month of a basin in its peak production is insufficient to characterize
739 emissions from an area that is likely to be producing and transporting gas at various intensities for decades. We need to quantify
740 the long-term climatological impacts of gas production. Future work examining the temporal variability of CH₄ emissions
741 within natural gas basins would complement short-term, high-intensity studies such as this one, and aid with understanding
742 how well the calculated emission rates represent the gas basin over the course of time.



743 **Acknowledgements**

744 This work has been funded by the U.S. Department of Energy National Energy Technology Laboratory (project DE-
745 FE0013590). We thank in-kind contributions from the Global Monitoring Division of the National Oceanic and Atmospheric
746 Administration, and from the Earth and Environmental Systems Institute, the Department of Meteorology and Atmospheric
747 Science, and the College of Earth and Mineral Science of The Pennsylvania State University. We also want to thank the
748 Pennsylvania College of Technology in Williamsport, PA for access to their Technology Aviation Center facilities during the
749 aircraft campaign. We also want to thank Lillie Langlois from the Department of Ecosystem Science and Management for
750 sharing pipeline information, Anthony J. Marchese and Dan Zimmerle (Colorado State University) for information on
751 compressor stations, Jeff Peischl for sharing data from his 2013 flight campaign, and Bernd Haupt (Penn State University) for
752 data processing and management during the project. Finally, we would like to thank Dennis and Joan Thomson for their
753 creation and continued support of the Thomson Distinguished Graduate Fellowship.

754 **References**

- 755 Alvarez, R. A., Pacala, S. W., Winebrake, J. J., Chameides, W. L., and Hamburg, S. P.: Greater focus needed on methane
 756 leakage from natural gas infrastructure, *Proceedings of the National Academy of Sciences*, 109, 6435-6440,
 757 10.1073/pnas.1202407109, 2012.
 758
- 759 Bloom, A. A., Bowman, K., Lee, M., Turner, A. J., Schroeder, R., Worden, J. R., Weidner, R., McDonald, K. C., and Jacob,
 760 D. J.: A global wetland methane emissions and uncertainty dataset for atmospheric chemical transport models, *Geosci.*
 761 *Model Dev. Discuss.*, doi:10.5194/gmd-2016-224, in review, 2016.
 762
- 763 Bradford County: Maps of Natural Gas Development in Bradford County, available at:
 764 <http://www.bradfordcountypa.org/index.php/natural-gas-information>.
 765
- 766 Bousquet, P., Ciais, P., Miller, J. B., Dlugokencky, E. J., Hauglustaine, D. A., Prigent, C., Van der Werf, G. R., Peylin, P.,
 767 Brunke, E. G., Carouge, C., Langenfelds, R. L., Lathiere, J., Papa, F., Ramonet, M., Schmidt, M., Steele, L. P., Tyler,
 768 S. C., and White, J.: Contribution of anthropogenic and natural sources to atmospheric methane variability, *Nature*,
 769 443, 439-443, http://www.nature.com/nature/journal/v443/n7110/supinfo/nature05132_S1.html, 2006.
 770
- 771 Brandt, A. R., Heath, G. A., Kort, E. A., O'Sullivan, F., Pétron, G., Jordaan, S. M., Tans, P., Wilcox, J., Gopstein, A. M., Arent,
 772 D., Wofsy, S., Brown, N. J., Bradley, R., Stucky, G. D., Eardley, D., and Harriss, R.: Methane Leaks from North
 773 American Natural Gas Systems, *Science*, 343, 733-735, 10.1126/science.1247045, 2014.
 774
- 775 Cambaliza, M. O. L., Shepson, P. B., Caulton, D. R., Stirm, B., Samarov, D., Gurney, K. R., Turnbull, J., Davis, K. J., Possolo,
 776 A., Karion, A., Sweeney, C., Moser, B., Hendricks, A., Lauvaux, T., Mays, K., Whetstone, J., Huang, J., Razlivanov,
 777 I., Miles, N. L., and Richardson, S. J.: Assessment of uncertainties of an aircraft-based mass balance approach for
 778 quantifying urban greenhouse gas emissions, *Atmos. Chem. Phys.*, 14, 9029-9050, 10.5194/acp-14-9029-2014, 2014.
 779
- 780 Chen, F., and Dudhia, J.: Coupling an Advanced Land Surface–Hydrology Model with the Penn State–NCAR MM5 Modeling
 781 System. Part I: Model Implementation and Sensitivity, *Monthly Weather Review*, 129, 569-585, 10.1175/1520-
 782 0493(2001)129<0569:caalsh>2.0.co;2, 2001.
 783
- 784 Conley, S., Franco, G., Faloona, I., Blake, D. R., Peischl, J., and Ryerson, T. B.: Methane emissions from the 2015 Aliso
 785 Canyon blowout in Los Angeles, CA, *Science*, 10.1126/science.aaf2348, 2016.
 786
- 787 Deng, A., Stauffer, D., Gaudet, B., Dudhia, J., Hacker, J., Bruyere, C., Wu, W., Vandenberghe, F., Liu, Y., and Bourgeois, A.:
 788 Update on WRF-ARW end-to-end multi-scale FDDA system, 10th Annual WRF Users' Workshop, Boulder, CO,
 789 June 23, 2009.
 790
- 791 Deng, A., Gaudet, B., Dudhia, J., and Alapaty, K.: Implementation and Evaluation of a New Shallow Convection Scheme in
 792 WRF, 94th American Meteorological Society Annual Meeting, Atlanta, GA, February 2-6, 2014.
 793
- 794 EIA: Annual Energy Outlook 2012 with Projections to 2035, available at:
 795 [http://www.eia.gov/forecasts/aeo/pdf/0383\(2012\).pdf](http://www.eia.gov/forecasts/aeo/pdf/0383(2012).pdf), 2012.
 796
- 797 EIA: Layer Information for Interactive State Maps, available at: https://www.eia.gov/maps/layer_info-m.cfm, 2015
 798
- 799 EIA: Shale in the United States, available at: https://www.eia.gov/energyexplained/index.cfm?page=natural_gas_where,
 800 2016a
 801



- 802 EIA: Monthly Energy Review: June 2016. [Available online at
 803 <http://www.eia.gov/totalenergy/data/monthly/archive/00351607.pdf> , 2016b.
 804
- 805 EPA: Abandoned Coal Mine Methane Opportunities Database, available at: [https://www.epa.gov/cmop/abandoned-](https://www.epa.gov/cmop/abandoned-underground-mines)
 806 [underground-mines](https://www.epa.gov/cmop/abandoned-underground-mines), 2008.
 807
- 808 EPA: Greenhouse Gas Reporting Program 2014, available at: [https://www.epa.gov/ghgreporting/ghg-reporting-program-data-](https://www.epa.gov/ghgreporting/ghg-reporting-program-data-sets)
 809 [sets](https://www.epa.gov/ghgreporting/ghg-reporting-program-data-sets), 2015a.
 810
- 811 EPA: Inventory of US Greenhouse Gas Emissions and Sinks: 1990-2013 Annex 3.6, available at:
 812 <https://www.epa.gov/ghgemissions/inventory-us-greenhouse-gas-emissions-and-sinks-1990-2013>, 2015b.
 813
- 814 EPA: Inventory of US Greenhouse Gas Emissions and Sinks: 1990-2014 Annex 2.2, available at:
 815 <https://www.epa.gov/ghgemissions/inventory-us-greenhouse-gas-emissions-and-sinks-1990-2014>, 2016.
 816
- 817 Frankenberg C., Thorpe, A. K., Thompson, D. R., Hulley, G., Kort, E. A., Vance, N., Borchardt, J., Krings, T., Gerilowski,
 818 K., Sweeney, C., Conley, S., Bue, B. D., Aubrey, A. D., Hook, S., and Green, R. O.: Airborne methane remote
 819 measurements reveal heavy-tail flux distribution in Four Corners region, *Proceedings of the National Academy of*
 820 *Sciences*, 113, 9734-9739, 2016.
 821
- 822 Hughes, J. D.: *Drilling Deeper: A Reality Check on US Government Forecasts for a Lasting Tight Oil & Shale Gas Boom*,
 823 *Post Carbon Institute*, Santa Rosa, California, 2014.
 824
- 825 Iacono, M. J., Delamere, J. S., Mlawer, E. J., Shephard, M. W., Clough, S. A., and Collins, W. D.: Radiative forcing by long-
 826 lived greenhouse gases: Calculations with the AER radiative transfer models, *Journal of Geophysical Research:*
 827 *Atmospheres*, 113, 10.1029/2008jd009944, 2008.
 828
- 829 Jimenez, P. A., Hacker, J. P., Dudhia, J., Haupt, S. E., Ruiz-Arias, J. A., Gueymard, C. A., Thompson, G., Eidhammer, T., and
 830 Deng, A.: WRF-Solar: Description and Clear-Sky Assessment of an Augmented NWP Model for Solar Power
 831 Prediction, *Bulletin of the American Meteorological Society*, 97, 1249-1264, 10.1175/bams-d-14-00279.1, 2016.
 832
- 833 Jiménez, P. A., Alessandrini, S., Haupt, S. E., Deng, A., Kosovic, B., Lee, J. A., and Monache, L. D.: The Role of Unresolved
 834 Clouds on Short-Range Global Horizontal Irradiance Predictability, *Monthly Weather Review*, 144, 3099-3107,
 835 10.1175/mwr-d-16-0104.1, 2016.
 836
- 837 Kain, J. S., and Fritsch, J. M.: A One-Dimensional Entraining/Detraining Plume Model and Its Application in Convective
 838 Parameterization, *Journal of the Atmospheric Sciences*, 47, 2784-2802, 10.1175/1520-
 839 0469(1990)047<2784:aodepm>2.0.co;2, 1990.
 840
- 841 Kain, J. S.: The Kain-Fritsch Convective Parameterization: An Update, *Journal of Applied Meteorology*, 43, 170-181,
 842 10.1175/1520-0450(2004)043<0170:tkcpau>2.0.co;2, 2004.
 843
- 844 Karion, A., Sweeney, C., Pétron, G., Frost, G., Michael Hardesty, R., Kofler, J., Miller, B. R., Newberger, T., Wolter, S.,
 845 Banta, R., Brewer, A., Dlugokencky, E., Lang, P., Montzka, S. A., Schnell, R., Tans, P., Trainer, M., Zamora, R., and
 846 Conley, S.: Methane emissions estimate from airborne measurements over a western United States natural gas field,
 847 *Geophysical Research Letters*, 40, 4393-4397, 10.1002/grl.50811, 2013.
 848
- 849 Karion, A., Sweeney, C., Kort, E. A., Shepson, P. B., Brewer, A., Cambaliza, M., Conley, S. A., Davis, K., Deng, A., Hardesty,
 850 M., Herndon, S. C., Lauvaux, T., Lavoie, T., Lyon, D., Newberger, T., Pétron, G., Rella, C., Smith, M., Wolter, S.,



- 851 Yacovitch, T. I., and Tans, P.: Aircraft-Based Estimate of Total Methane Emissions from the Barnett Shale Region,
852 Environmental Science & Technology, 49, 8124-8131, 10.1021/acs.est.5b00217, 2015.
853
- 854 Lamb, B. K., Cambaliza, M. O. L., Davis, K. J., Edburg, S. L., Ferrara, T. W., Floerchinger, C., Heimbürger, A. M. F., Herndon,
855 S., Lauvaux, T., Lavoie, T., Lyon, D. R., Miles, N., Prasad, K. R., Richardson, S., Roscioli, J. R., Salmon, O. E.,
856 Shepson, P. B., Stirm, B. H., and Whetstone, J.: Direct and Indirect Measurements and Modeling of Methane
857 Emissions in Indianapolis, Indiana, Environmental Science & Technology, 50, 8910-8917, 10.1021/acs.est.6b01198,
858 2016.
859
- 860 Lauvaux, T., Uliasz, M., Sarrat, C., Chevallier, F., Bousquet, P., Lac, C., Davis, K. J., Ciais, P., Denning, A. S., and Rayner,
861 P. J.: Mesoscale inversion: first results from the CERES campaign with synthetic data, Atmos. Chem. Phys., 8, 3459-
862 3471, 10.5194/acp-8-3459-2008, 2008.
863
- 864 Maasackers, J. D., Jacob, D. J., Sulprizio, M. P., Turner, A. J., Weitz, M., Wirth, T., Hight, C., DeFigueiredo, M., Desai, M.,
865 Schmeltz, R., Hockstad, L., Bloom, A. A., Bowman, K. W., Jeong, S., and Fischer, M. L.: Gridded National Inventory
866 of U.S. Methane Emissions, Environmental Science & Technology, 50, 13123-13133, 10.1021/acs.est.6b02878,
867 2016.
868
- 869 Marchese, A. J., Vaughn, T. L., Zimmerle, D. J., Martinez, D. M., Williams, L. L., Robinson, A. L., Mitchell, A. L.,
870 Subramanian, R., Tkacik, D. S., Roscioli, J. R., and Herndon, S. C.: Methane Emissions from United States Natural
871 Gas Gathering and Processing, Environmental Science & Technology, 49, 10718-10727, 10.1021/acs.est.5b02275,
872 2015.
873
- 874 Mays, K. L., Shepson, P. B., Stirm, B. H., Karion, A., Sweeney, C., and Gurney, K. R.: Aircraft-Based Measurements of the
875 Carbon Footprint of Indianapolis, Environmental Science & Technology, 43, 7816-7823, 10.1021/es901326b, 2009.
876
- 877 Mlawer, E. J., Taubman, S. J., Brown, P. D., Iacono, M. J., and Clough, S. A.: Radiative transfer for inhomogeneous
878 atmospheres: RRTM, a validated correlated-k model for the longwave, Journal of Geophysical Research:
879 Atmospheres, 102, 16663-16682, 10.1029/97jd00237, 1997.
880
- 881 Myhre, G., Shindell, D., Bréon, F.-M., Collins, W., Fuglestedt, J., Huang, J., Koch, D., Lamarque, J.-F., Lee, D., and
882 Mendoza, B.: Anthropogenic and natural radiative forcing, Climate change, 423, 2013.
883
- 884 Nakanishi, M., and Niino, H.: An improved Mellor–Yamada level-3 model: Its numerical stability and application to a regional
885 prediction of advection fog, Boundary-Layer Meteorology, 119, 397-407, 2006.
886
- 887 NYDEC: NY 2014 Oil & Gas Production Data: available at: <http://www.dec.ny.gov/energy/36159.html>, 2016.
888
- 889 Omara, M., Sullivan, M. R., Li, X., Subramanian, R., Robinson, A. L., and Presto, A. A.: Methane Emissions from
890 Conventional and Unconventional Natural Gas Production Sites in the Marcellus Shale Basin, Environmental Science
891 & Technology, 50, 2099-2107, 10.1021/acs.est.5b05503, 2016.
892
- 893 Overend, R. P., Paraskevopoulos, G., and Cvetanović, R. J.: Rates of OH Radical Reactions. I. Reactions with H₂, CH₄, C₂H₆,
894 and C₃H₈ at 295 K, Canadian Journal of Chemistry, 53, 3374-3382, 10.1139/v75-482, 1975.
895
- 896 PADEP: PA Oil and Gas Well Historical Production Report, available at:
897 http://www.depreportingservices.state.pa.us/ReportServer/Pages/ReportViewer.aspx?%2fOil_Gas%2fOil_Gas_Wel
898 [l_Historical_Production_Report](http://www.depreportingservices.state.pa.us/ReportServer/Pages/ReportViewer.aspx?%2fOil_Gas_Wel), 2016.
899



- 900 Peischl, J., Ryerson, T. B., Aikin, K. C., de Gouw, J. A., Gilman, J. B., Holloway, J. S., Lerner, B. M., Nadkarni, R., Neuman,
 901 J. A., Nowak, J. B., Trainer, M., Warneke, C., and Parrish, D. D.: Quantifying atmospheric methane emissions from
 902 the Haynesville, Fayetteville, and northeastern Marcellus shale gas production regions, *Journal of Geophysical*
 903 *Research: Atmospheres*, 120, 2119-2139, 10.1002/2014jd022697, 2015.
- 904
- 905 Pétron, G., Frost, G., Miller, B. R., Hirsch, A. I., Montzka, S. A., Karion, A., Trainer, M., Sweeney, C., Andrews, A. E., Miller,
 906 L., Kofler, J., Bar-Ilan, A., Dlugokencky, E. J., Patrick, L., Moore, C. T., Ryerson, T. B., Siso, C., Kolodzey, W.,
 907 Lang, P. M., Conway, T., Novelli, P., Masarie, K., Hall, B., Guenther, D., Kitzis, D., Miller, J., Welsh, D., Wolfe, D.,
 908 Neff, W., and Tans, P.: Hydrocarbon emissions characterization in the Colorado Front Range: A pilot study, *Journal*
 909 *of Geophysical Research: Atmospheres*, 117, n/a-n/a, 10.1029/2011jd016360, 2012.
- 910
- 911 Platts: Maps and Geospatial Data: available at: <http://www.platts.com/maps-geospatial>, 2016.
- 912
- 913 Rogers, R., Deng, A., Stauffer, D., Jia, Y., Soong, S., Tanrikulu, S., Beaver, S., and Tran, C.: Fine particulate matter modeling
 914 in Central California. Part I: Application of the Weather Research and Forecasting model, 91th Annual Meeting,
 915 2011.
- 916
- 917 Ryerson, T. B., Trainer, M., Holloway, J. S., Parrish, D. D., Huey, L. G., Sueper, D. T., Frost, G. J., Donnelly, S. G., Schauffler,
 918 S., Atlas, E. L., Kuster, W. C., Goldan, P. D., Hübler, G., Meagher, J. F., and Fehsenfeld, F. C.: Observations of
 919 Ozone Formation in Power Plant Plumes and Implications for Ozone Control Strategies, *Science*, 292, 719-723,
 920 10.1126/science.1058113, 2001.
- 921
- 922 Schwietzke, S., Griffin, W. M., Matthews, H. S., and Bruhwiler, L. M. P.: Natural Gas Fugitive Emissions Rates Constrained
 923 by Global Atmospheric Methane and Ethane, *Environmental Science & Technology*, 48, 7714-7722,
 924 10.1021/es501204c, 2014.
- 925
- 926 Smith, M. L., Kort, E. A., Karion, A., Sweeney, C., Herndon, S. C., and Yacovitch, T. I.: Airborne Ethane Observations in the
 927 Barnett Shale: Quantification of Ethane Flux and Attribution of Methane Emissions, *Environmental Science &*
 928 *Technology*, 49, 8158-8166, 10.1021/acs.est.5b00219, 2015.
- 929
- 930 Skamarock, W. C., Klemp, J. B., Dudhia, J., Gill, D. O., Barker, D. M., Wang, W., and Powers, J. G.: A description of the
 931 advanced research WRF version 2, DTIC Document, 2005.
- 932
- 933 Stone, D., Whalley, L. K., and Heard, D. E.: Tropospheric OH and HO₂ radicals: field measurements and model comparisons,
 934 *Chemical Society Reviews*, 41, 6348-6404, 10.1039/c2cs35140d, 2012.
- 935
- 936 Tewari, M., Chen, F., Wang, W., Dudhia, J., LeMone, M., Mitchell, K., Ek, M., Gayno, G., Wegiel, J., and Cuenca, R.:
 937 Implementation and verification of the unified NOAH land surface model in the WRF model, 20th conference on
 938 weather analysis and forecasting/16th conference on numerical weather prediction, 2004.
- 939
- 940 Thompson, G., Field, P. R., Rasmussen, R. M., and Hall, W. D.: Explicit Forecasts of Winter Precipitation Using an Improved
 941 Bulk Microphysics Scheme. Part II: Implementation of a New Snow Parameterization, *Monthly Weather Review*,
 942 136, 5095-5115, 10.1175/2008mwr2387.1, 2008.
- 943
- 944 USDA: Census Ag Atlas Maps, available at:
 945 https://www.agcensus.usda.gov/Publications/2012/Online_Resources/Ag_Atlas_Maps/Livestock_and_Animals/,
 946 2012.
- 947
- 948 White, W. H., Anderson, J. A., Blumenthal, D. L., and Wilson, W. E.: Formation and transport of secondary air-pollutants:
 949 Ozone and aerosols in St. Louis urban plume: *Science* 194, 187-189, 10.1126/science.959846, 1976.



- 950
951 WVDEP: WV Oil and Gas Database and Map Information, available at: <http://www.dep.wv.gov/oil-and->
952 [gas/databaseinfo/Pages/default.aspx](http://www.dep.wv.gov/oil-and-gas/databaseinfo/Pages/default.aspx), 2016.
953
954 Zavala-Araiza, D., Lyon, D., Alvarez, R. A., Palacios, V., Harriss, R., Lan, X., Talbot, R., and Hamburg, S. P.: Toward a
955 Functional Definition of Methane Super-Emitters: Application to Natural Gas Production Sites, Environmental
956 Science & Technology, 49, 8167-8174, 10.1021/acs.est.5b00133, 2015
957
958 Zavala-Araiza, D., Alvarez, R. A., Lyon, D. R., Allen, D. T., Marchese, A. J., Zimmerle, D. J., and Hamburg, S. P.: Super-
959 emitters in natural gas infrastructure are caused by abnormal process conditions, Nature Communications, 8, 14012,
960 10.1038/ncomms14012, 2017.
961
962 Zimmerle, D. J., Williams, L. L., Vaughn, T. L., Quinn, C., Subramanian, R., Duggan, G. P., Willson, B., Opsomer, J. D.,
963 Marchese, A. J., Martinez, D. M., and Robinson, A. L.: Methane Emissions from the Natural Gas Transmission and
964 Storage System in the United States, Environmental Science & Technology, 49, 9374-9383, 10.1021/acs.est.5b01669,
965 2015.

**Table 1: List of tracers used in the transport model.**

Tracer #	Name	Description of source
1	Unconventional Wells	Emissions from unconventional wells.
2	Storage Facilities	Emissions from compressors associated with natural gas storage.
3	Pipelines	Emissions from gathering and transmission pipelines
4	Distribution	Emissions from the distribution sector of the natural gas industry.
5	Conventional Wells	Emissions from conventional wells.
6	Landfills/Other	Emissions from landfills and uncharacterized industrial sources.
7	Coal	Emissions from active and abandoned coal mining.
8	Animals/Waste	Emissions from enteric fermentation and manure management
9	Production Compressors (HP)	Emissions from compressor stations characterized as “production”. Emissions scaled linearly with wattage.
10	Gathering Compressors (HP)	Emissions from compressor stations characterized as “gathering”. Emissions scaled linearly with wattage.
11	Other Compressors (HP)	Emissions from all other compressor stations. Emissions scaled linearly with wattage.
12	Production Compressors (C)	Emissions from compressor stations characterized as “production”. Emissions constant among compressors.
13	Gathering Compressors (C)	Emissions from compressor stations characterized as “gathering”. Emissions constant among compressors.
14	Other Compressors (C)	Emissions from all other compressor stations. Emissions constant among compressors.



Table 2: Annual emission rate totals from anthropogenic sources within the innermost model domain based on values from the inventory within this study

Source	Total Emission Rate (Gg CH ₄ year ⁻¹)
Unconventional Wells	125
Conventional Wells	607
Gathering Compressor Facilities	118
Storage Facilities	69
Gathering/Transmission Pipelines	8
Natural Gas Distribution	213
Underground, Surface, and Abandoned Coal Mines	831
Enteric Fermentation/Manure Management	371
Landfills	420
Total	2762

Table 3: Meteorological statistics from the May 2015 flight campaign.

Day	Flight Pattern	# of Loops	# of Vertical Profiles	ABL Depth (m)	Mean Observed Wind Speed (m/s)	Mean Observed Wind Direction	Model Background Value (ppm)
May 14	Box	1	2	1300	2.9	30°	1.908
May 21	Raster	N/A	2	1300	3.9	231°	1.905
May 22	Box	2	2	2300	10.1	300°	1.910
May 23	Box	2	2	1400	4.4	276°	1.906
May 24 ¹	Other	N/A	2	1500	4.4	270°	1.923
May 24 ²	Raster	N/A	2	2050	4.8	272°	1.907
May 25	Box	1	2	1800	9.0	217°	1.920
May 28	Box	2	3	1400	7.1	322°	1.897
May 29	Box	2	2	1000	4.6	195°	1.899
June 3	Raster	N/A	1	1250	2.7	149°	1.898



Table 4: Optimized natural gas emission rates for each flight as well as corrected emission rates adjusting for errors in the model wind speed and boundary layer height. For wind speed and boundary layer height error, a negative value represents a model value less than the observations.

Day	Optimized NG Emission Rate (% of production)	Wind Speed Error (6)	Boundary Layer Height Error (7)	Corrected NG Emission Rate (% of production)
May 14	0.37	-31%	-33%	0.17
May 21	0.53	3%	39%	0.76
May 22	1.15	37%	-18%	1.30
May 23	0.45	34%	-9%	0.55
May 24	0.68	48%	-21%	0.80
May 24	0.36	48%	-21%	0.42
May 25	0.99	3%	-43%	0.58
May 28	0.33	-4%	-8%	0.29
May 29	0.35	4%	1%	0.37
June 3	0.26	19%	-8%	0.29
Average	0.55	16%	-12%	0.55

Table 5: Emission rates and potential errors associated with the model optimization technique

Day	Optimized Upstream Emission Rate (% of production)	Background Error	Non-Upstream Gas Inventory Error	Model Performance Error	Total Error	2 σ Confidence Interval (% of Production)
May 14	0.37	$\pm 24\%$	$\pm 20\%$	$\pm 17\%$	$\pm 36\%$	± 0.13
May 21	0.53	$\pm 24\%$	$\pm 17\%$	$\pm 30\%$	$\pm 42\%$	± 0.22
May 22	1.15	$\pm 38\%$	$\pm 6\%$	$\pm 37\%$	$\pm 53\%$	± 0.61
May 23	0.45	$\pm 39\%$	$\pm 13\%$	$\pm 42\%$	$\pm 59\%$	± 0.26
May 24 ¹	0.68	$\pm 24\%$	$\pm 54\%$	$\pm 17\%$	$\pm 61\%$	± 0.42
May 24 ²	0.36	$\pm 51\%$	$\pm 78\%$	$\pm 31\%$	$\pm 98\%$	± 0.35
May 25	0.99	$\pm 29\%$	$\pm 19\%$	$\pm 30\%$	$\pm 46\%$	± 0.45
May 28	0.33	$\pm 76\%$	$\pm 36\%$	$\pm 20\%$	$\pm 86\%$	± 0.29
May 29	0.35	$\pm 24\%$	$\pm 9\%$	$\pm 19\%$	$\pm 32\%$	± 0.11
June 3	0.26	$\pm 31\%$	$\pm 10\%$	$\pm 24\%$	$\pm 40\%$	± 0.11



Table 6: Emission rates from mass balance calculations on applicable days, with emission ranges associated with a ± 5 ppb error in the background value.

Flight	CH ₄ Production within box (Gg hr ⁻¹)	Mass Balance CH ₄ Flux (kg hr ⁻¹)	Non-Upstream CH ₄ Emissions (kg hr ⁻¹)	Calculated Upstream Emission Rate (% of production)	2 σ Confidence Interval (% of Production)
May 22 ₁	4.96	53800	2250	1.04	± 1.09
May 22 ₂	4.96	27400	2250	0.51	± 1.08
May 23 ₁	4.05	5600	934	0.11	± 0.07
May 23 ₂	4.05	5500	934	0.11	± 0.07
May 28 ₁	3.73	7100	706	0.17	± 0.11
May 28 ₂	3.73	6000	843	0.14	± 0.10
May 29 ₁	4.63	27900	1622	0.57	± 0.30

**Table 7: Relative error associated with the different sources of uncertainty.**

Flight	Wind Speed Error	Background Error	ABL Error	Inventory Error	Total Error (1σ)	Upstream Emission Rate (% of Production) w/ 2σ Confidence Interval
May 22 ₁	±3%	±56%	±9%	±5%	±57%	1.04 ±1.09
May 22 ₂	±3%	±121%	±9%	±8%	±121%	0.51 ±1.08
May 23 ₁	±3%	±24%	±7%	±20%	±32%	0.11 ±0.07
May 23 ₂	±3%	±26%	±7%	±21%	±34%	0.11 ±0.07
May 28 ₁	±3%	±31%	±7%	±11%	±34%	0.17 ±0.11
May 28 ₂	±3%	±33%	±7%	±16%	±38%	0.14 ±0.10
May 29 ₁	±3%	±28%	±20%	±8%	±36%	0.57 ±0.30

Table 8: Production statistics from mid-2014 for various shales across the United States (Hughes 2014).

	Barnett	Fayetteville	Haynesville	Marcellus	Bradford/ Susquehanna County, PA
# of Producing Wells	16100	4500	3100	7000	1558
Total Production (Bcf day ⁻¹)	5.0	2.8	4.5	12	5.01
Production per well (MMcf day ⁻¹)	0.31	0.56	1.25	1.71	3.22

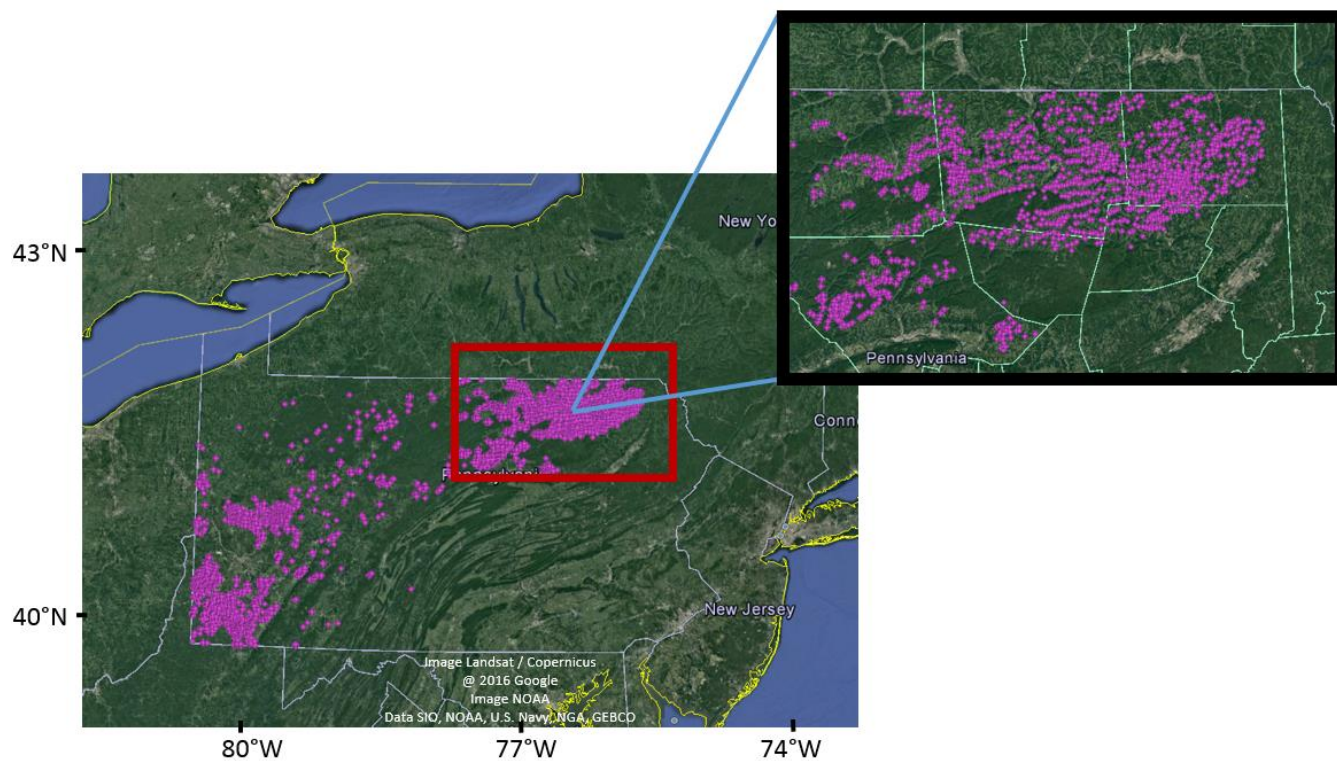


Figure 1: A map of the unconventional wells in Pennsylvania dotted in purple. Red rectangle and zoom-in show the region of focus for this study, 41.1-42.2°N 75.2-77.6°W.

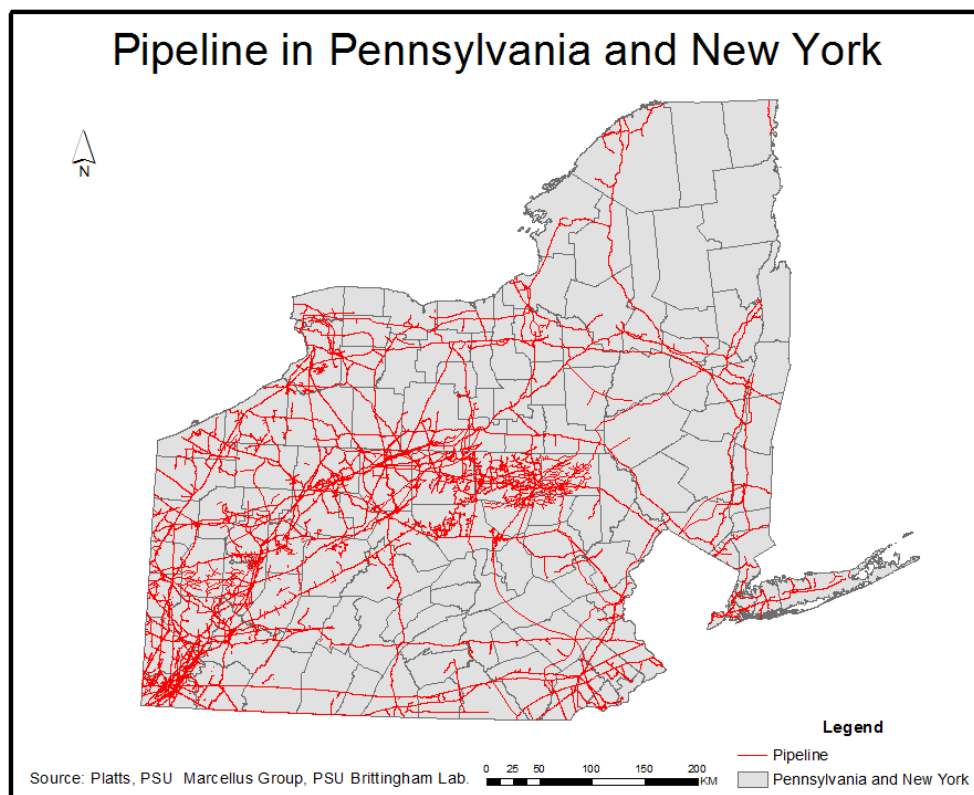


Figure 2: A map of transmission and gathering pipelines for the state of PA and NY. Transmission pipelines are provided by Platts Natural Gas Pipelines product. Gathering pipelines associated with unconventional wells in PA are extrapolated using information on existing gathering pipelines provided by Bradford County, PA.

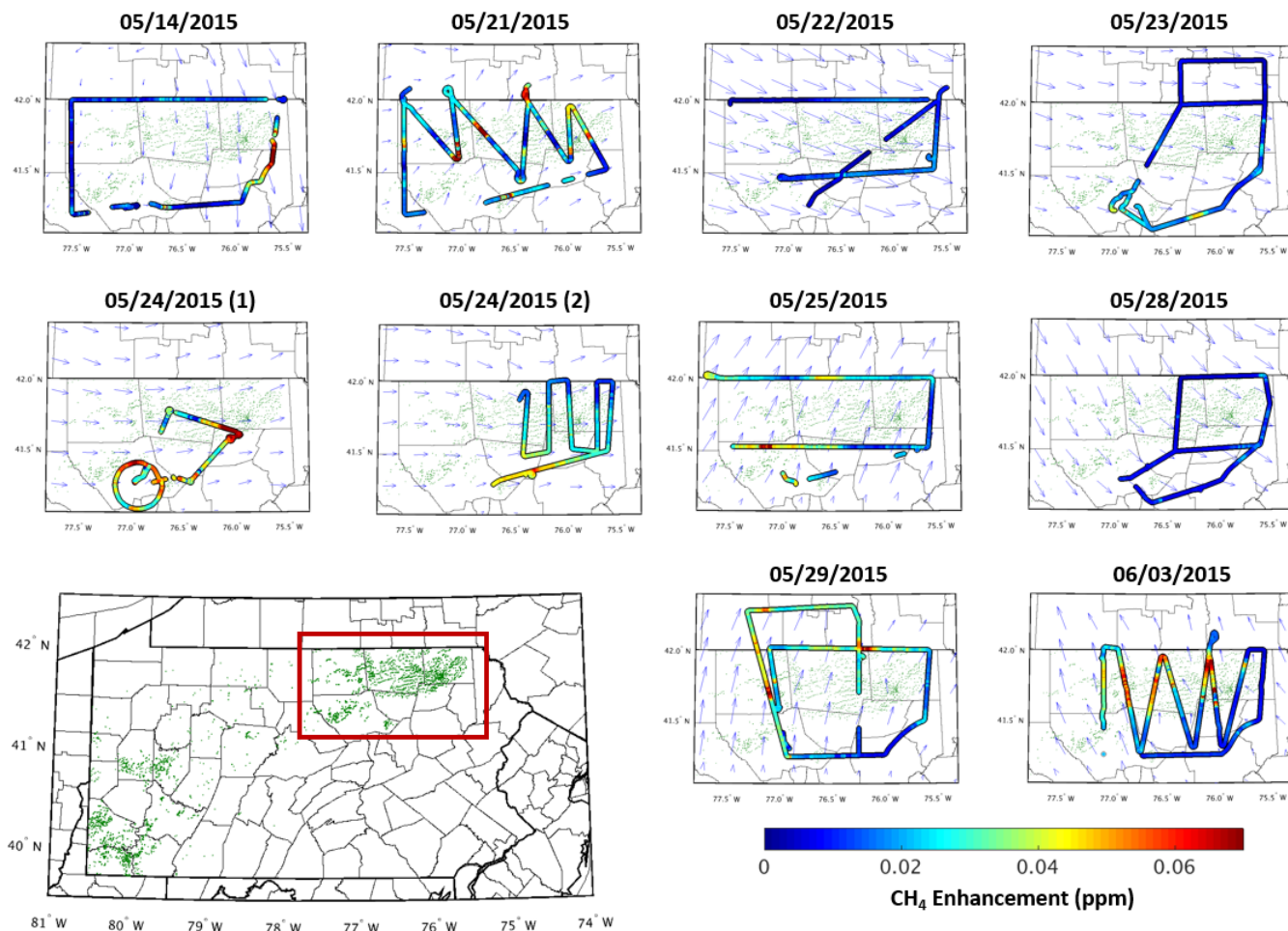


Figure 3: Observed CH_4 enhancements within the boundary layer from each of the 10 afternoon flights used in this study, with green dots showing the location of unconventional wells in PA and blue arrows showing the modelled wind direction during the time of the flight. CH_4 enhancements are calculated by taking the observed CH_4 mole fraction values and subtracting off the flight's background CH_4 value shown in Table 3.

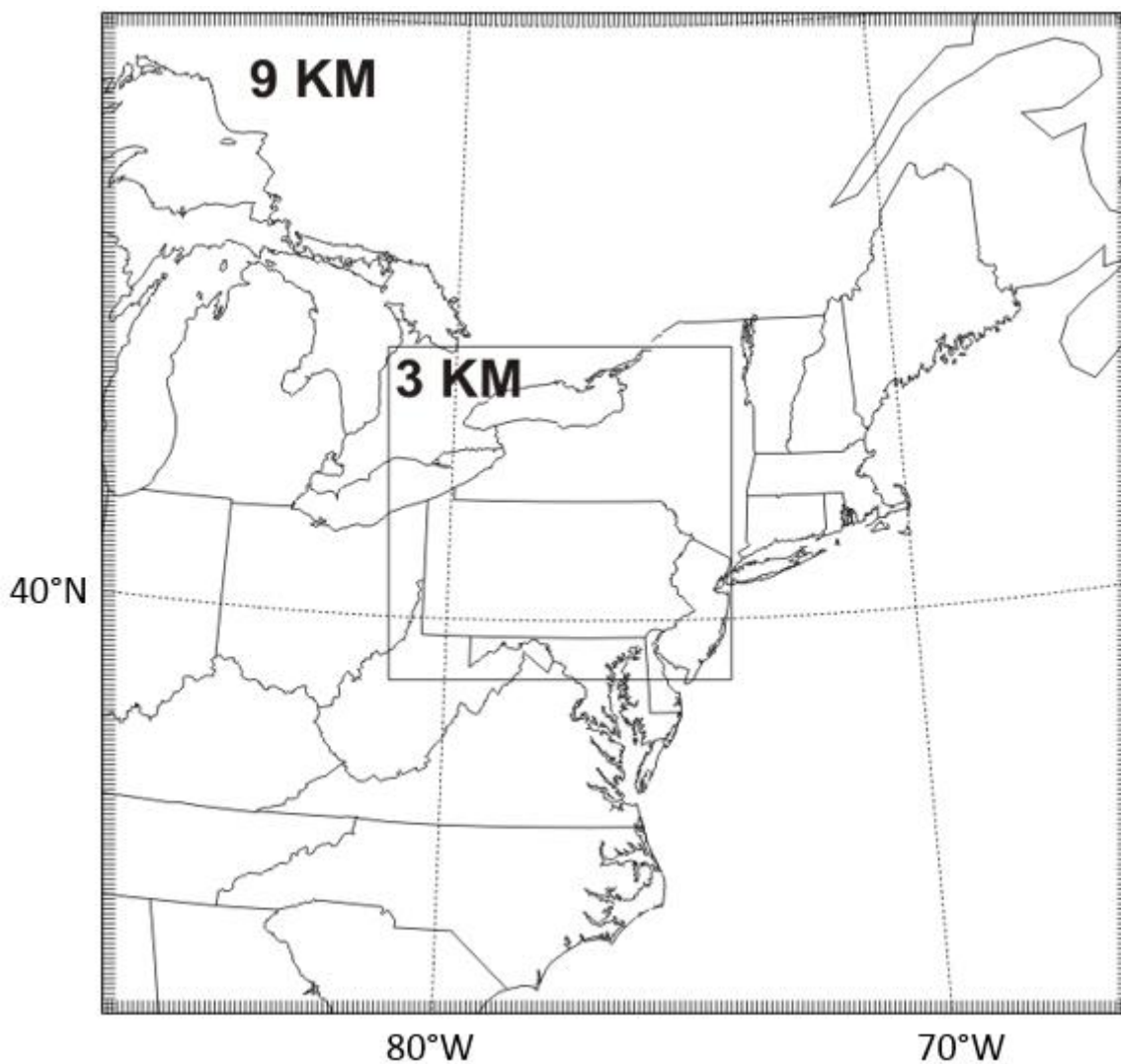


Figure 4: Model domain and resolutions used within the transport model. All emissions used for this study are contained within the 3 km resolution domain.

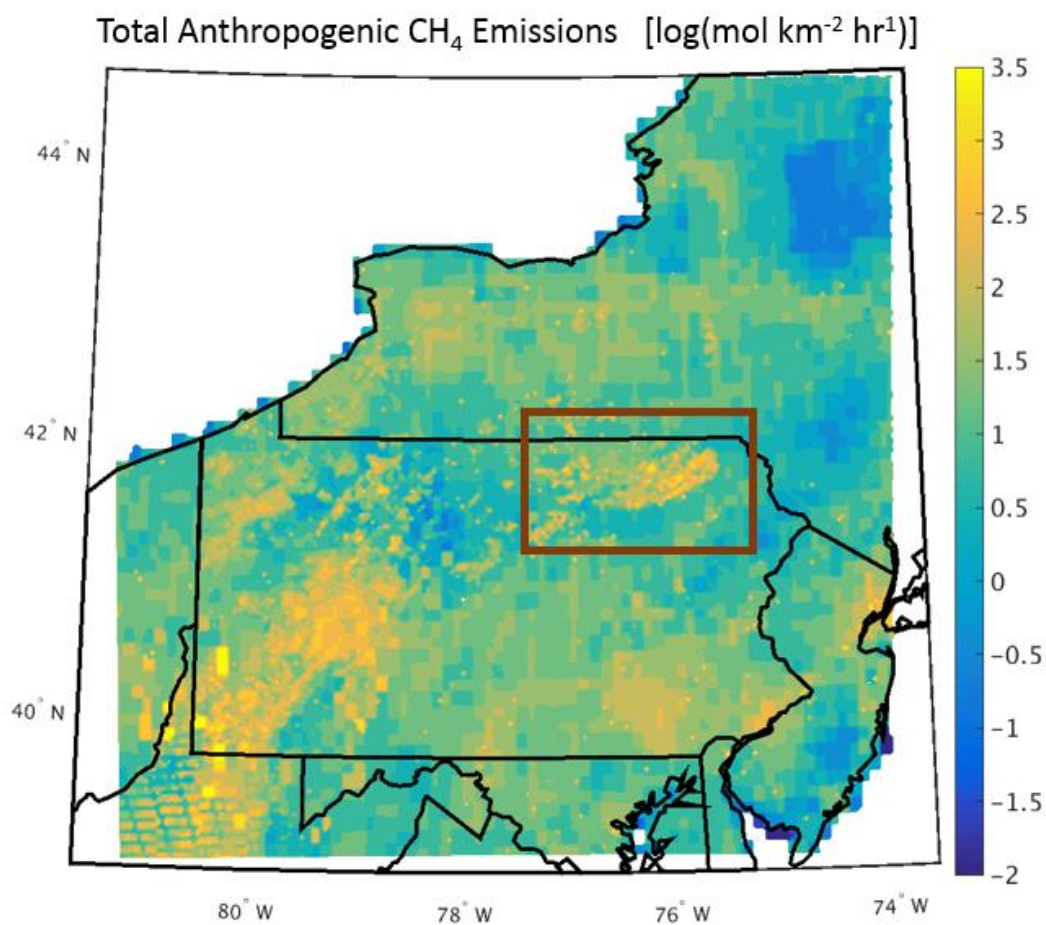


Figure 5: A log scale contour of the anthropogenic CH₄ emissions inventory from this study used within the transport model. The red rectangle surrounds the study region where the aircraft campaign took place.

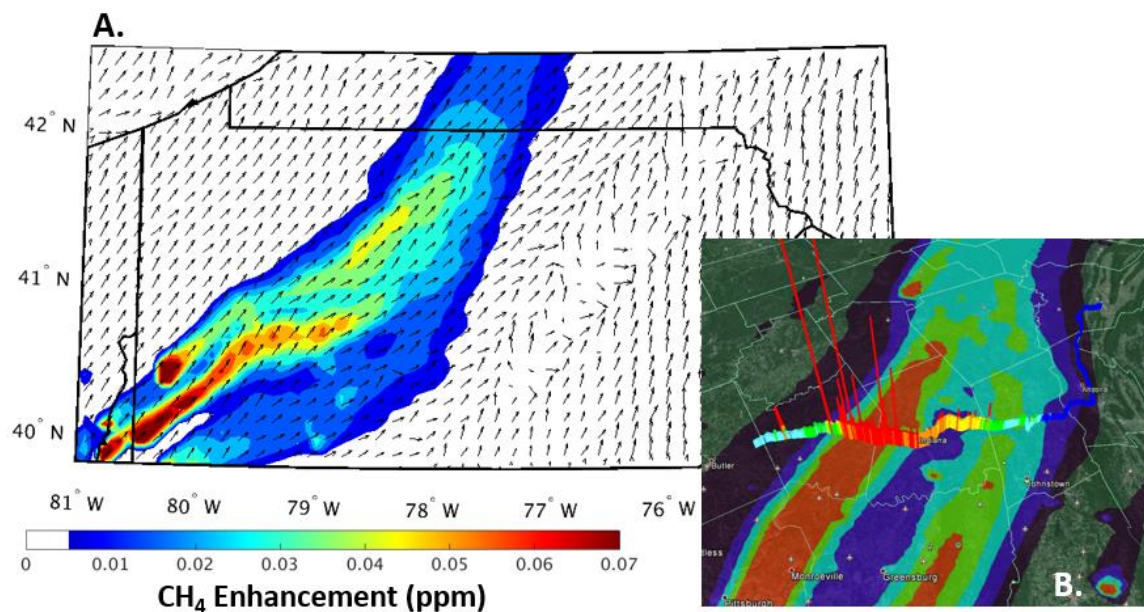


Figure 6: (a.) Model projected CH₄ enhancement at the surface associated with underground, surface, and abandoned coal mines on May 27th, 2015 at 19Z, with the shaded regions showing the CH₄ enhancement and the arrows representing the wind direction. (b.) Projected enhancement from a. mapped over measured CH₄ enhancement from a driving campaign. The height and colour of the bars represents the scale of the CH₄ enhancement.

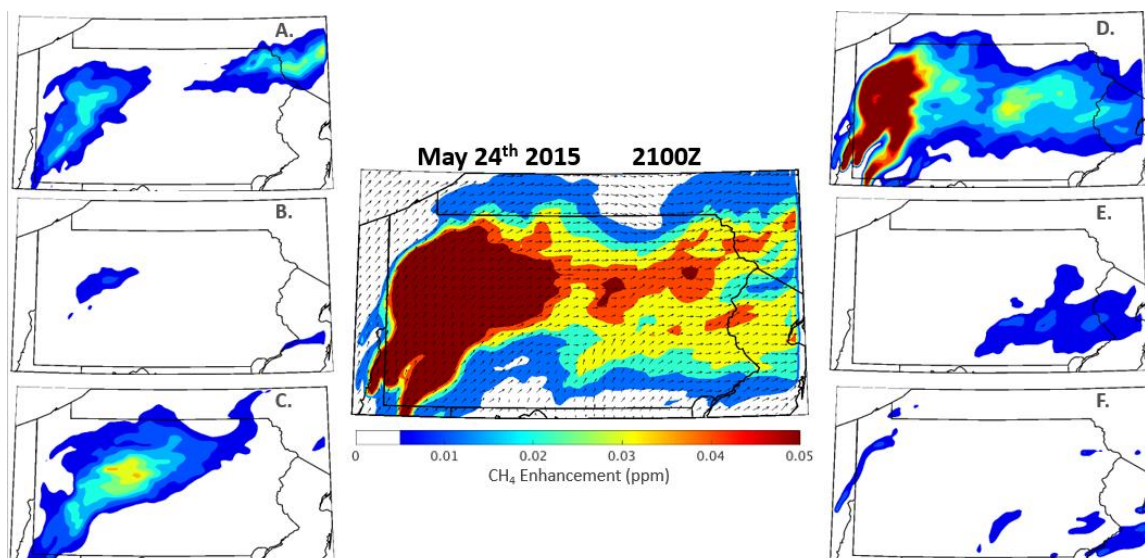


Figure 7: Projected CH₄ enhancements during the late afternoon flight of May 24th, 2015 at 2100Z, 700m above ground level from (A) upstream unconventional gas processes (B) downstream unconventional gas processes (C) conventional production (D) coal mines (E) animal emissions and (F) landfills and other sources within the EPA GHG Inventory Report. The centre figure is a map of the combined enhancement from sources A-F.

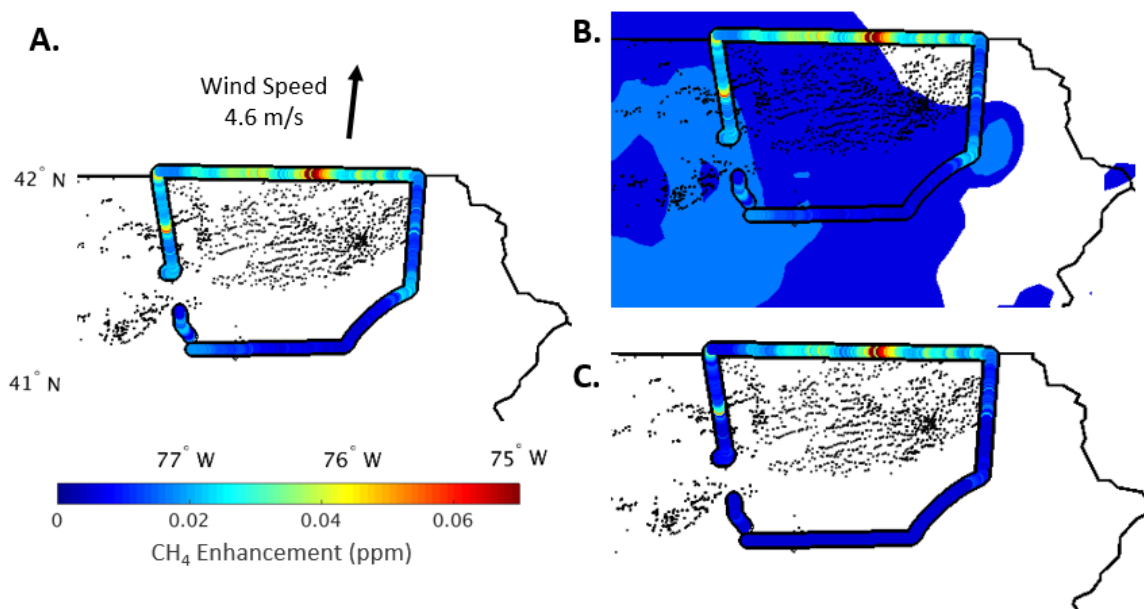


Figure 8: (a.) Observed CH₄ enhancements from within the boundary layer during the first loop of the May 29th aircraft campaign. (b.) Aircraft observations laid overtop modelled CH₄ concentrations from sources unrelated to emissions from upstream gas production. (c.) Observed CH₄ enhancements from the May 29th flight after subtracting off modelled sources in b. The new set of observations represent the observed upstream gas enhancement during the flight.

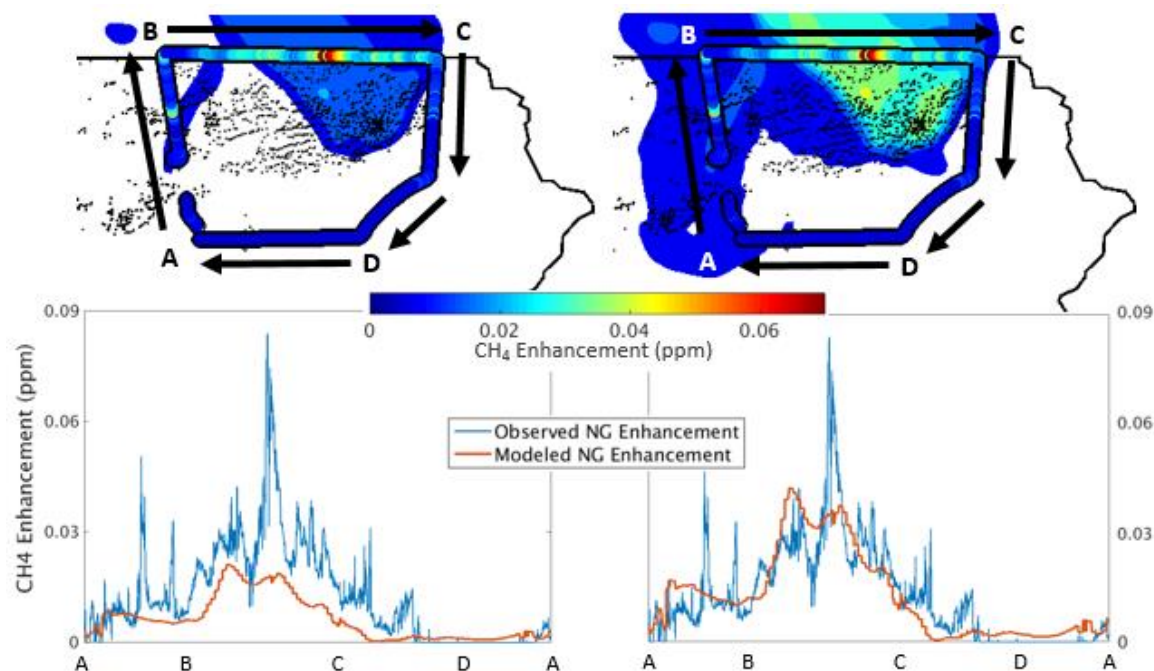


Figure 9: (top-left) Observed enhancement from unconventional natural gas production overtop projected upstream natural gas enhancements from the first loop of the May 29th flight, using an upstream gas emission rate of 0.13% of production. (bottom-left) Direct comparison of the observed natural gas enhancement vs. the modelled enhancement following the path from A-D using an unconventional emission rate of 0.13%. (top-right, bottom-right). Same as left figures, except using the optimized upstream emission rate of 0.26%

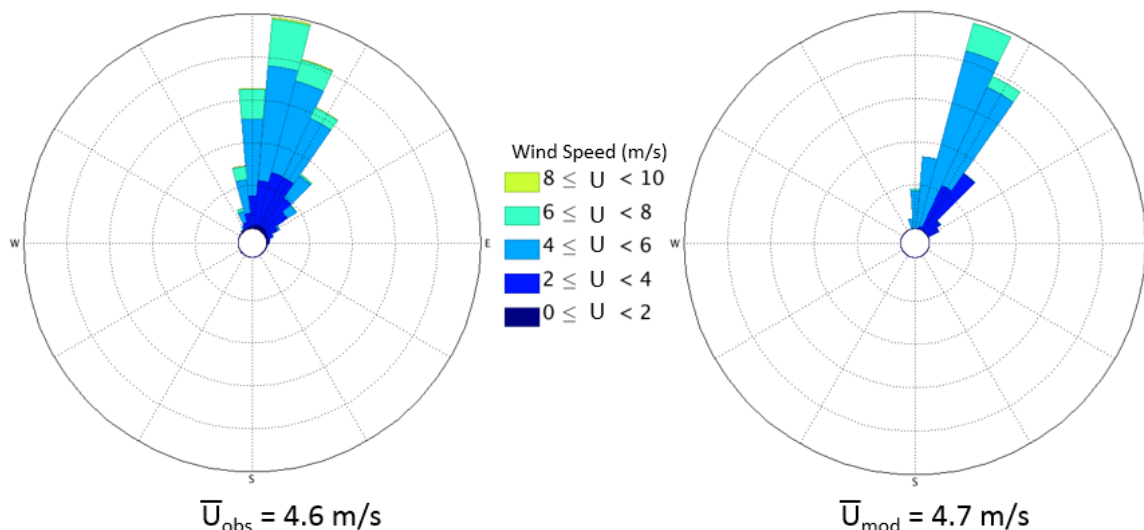


Figure 10: Wind rose of aircraft observations (left) within the boundary from the first loop of the May 29th flight compared to modelled winds following the flight path (right).

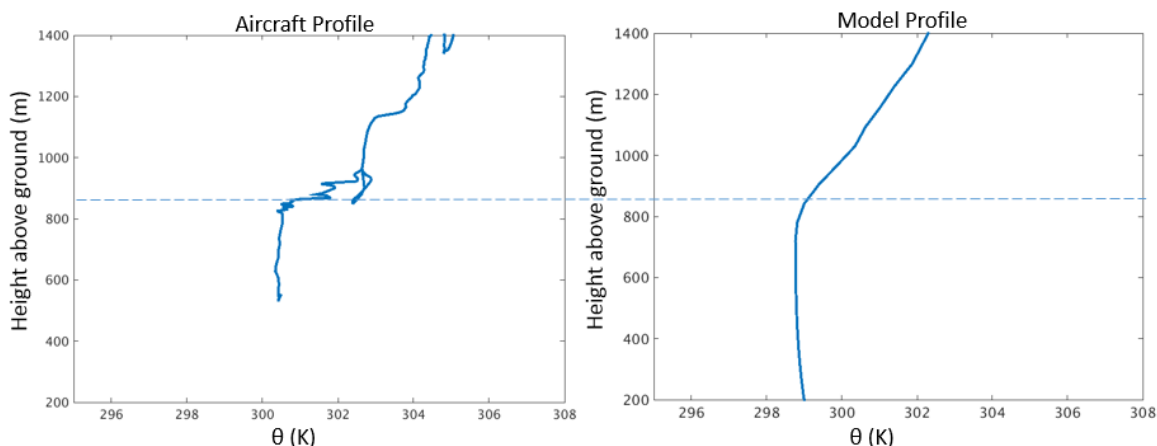


Figure 11: (left) Observed potential temperature profile with height from the first aircraft spiral on the May 29th flight at 17Z. (right) Modelled potential temperature at the location and time at which the aircraft spiral occurred. In both cases, an inversion in the potential temperature profile begins to occur around 850m.

May 24th 2015: Late-Afternoon Flight

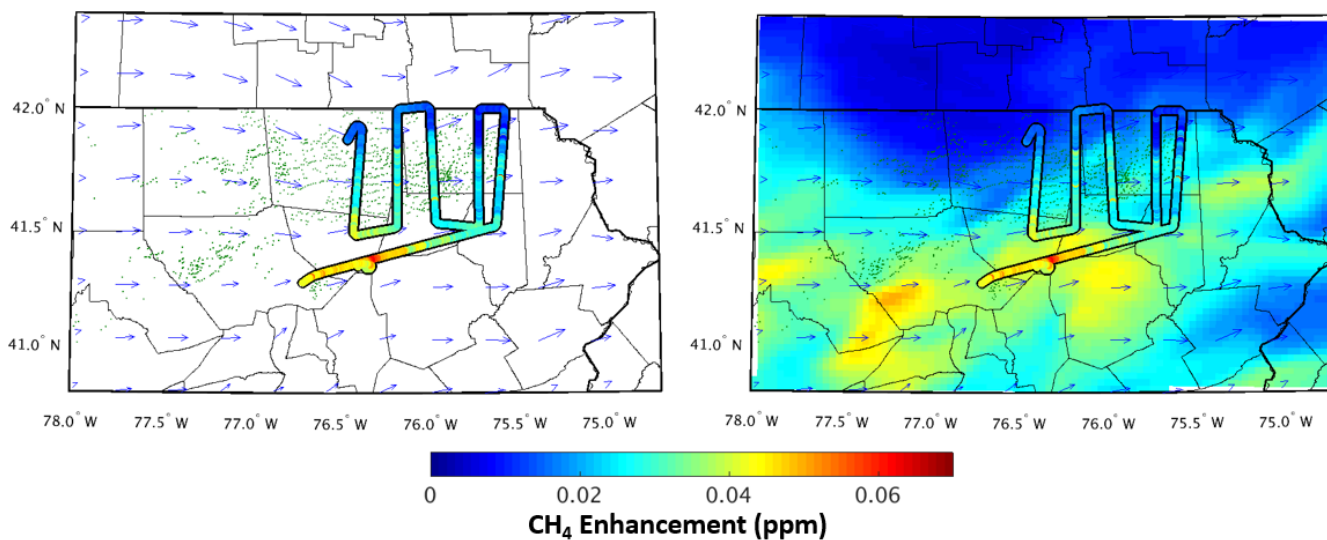


Figure 12: (left) Observed CH₄ enhancement from the late-afternoon flight on May 24th, 2015. (right) Observed CH₄ enhancement compared to the model projected CH₄ enhancement from the sum of all sources in the region. The colour scale of observed and projected enhancements is scaled 1:1, with matching colours indicating matching values.

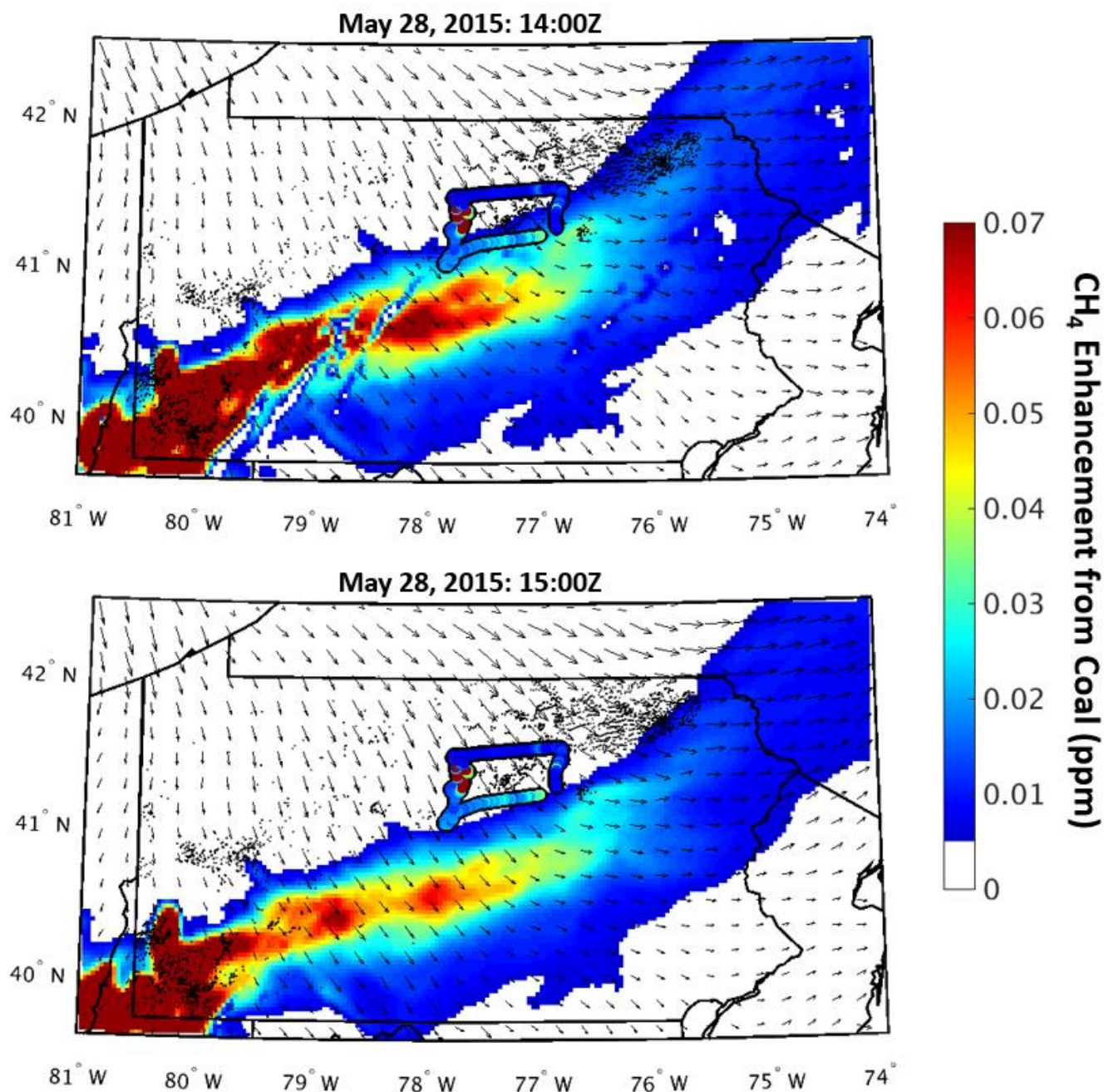


Figure 13: Observed CH₄ enhancements from an early flight on May 28th, 2015 compared to projected CH₄ enhancements from coal emissions modelled at (top) 14:00Z and (bottom) 15:00Z. The one hour time difference results in vastly different projected enhancements across the southern portion of observations.

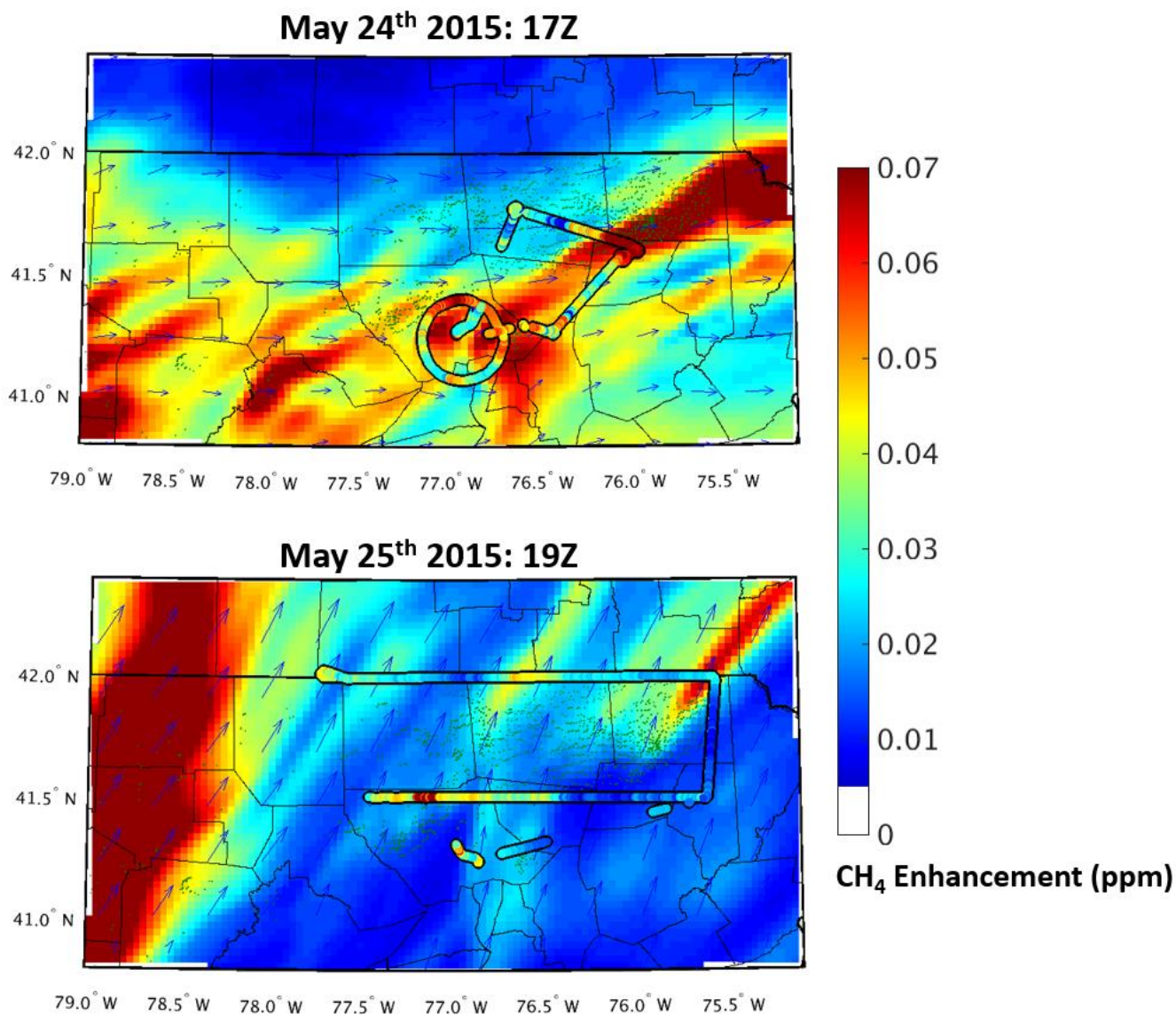


Figure 14: Observed vs model projected CH₄ enhancements during (top) the early afternoon flight of May 24th, 2015 at 17Z and (bottom) the flight of May 25th, 2016 at 19Z.

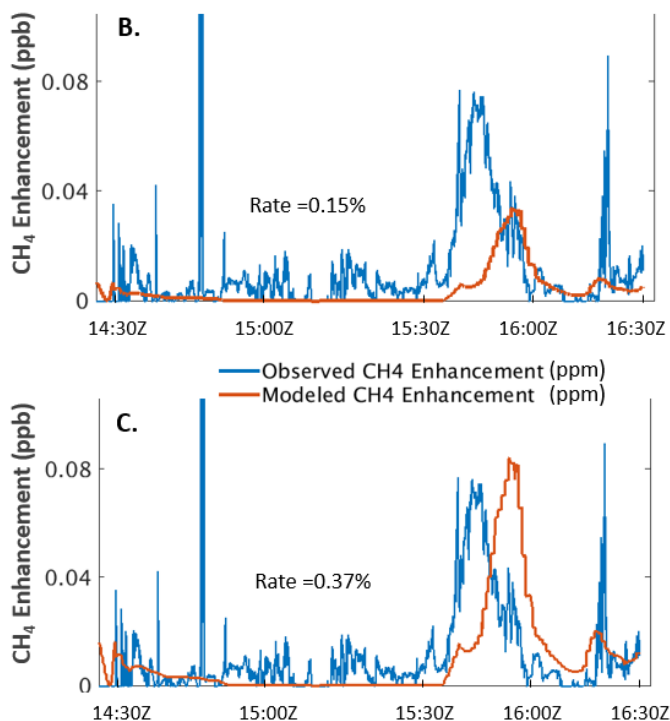
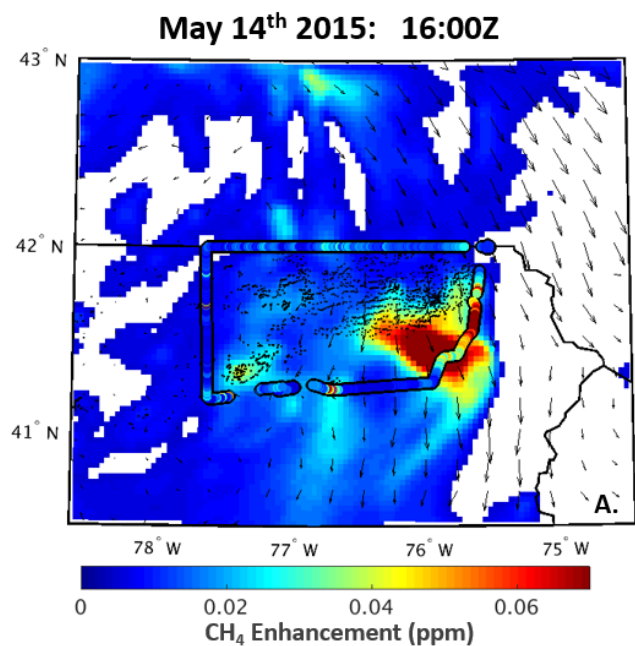


Figure 15: (a.) Observed vs model projected CH₄ enhancements during the May 14th, 2015 at 16Z. (b.) Comparison of observed natural gas enhancement to modelled natural gas enhancement along flight path, with upstream emission rate optimized by minimizing the absolute error between the datasets. (c.) Same as previous, but optimized by minimizing the sum of the error between the datasets.

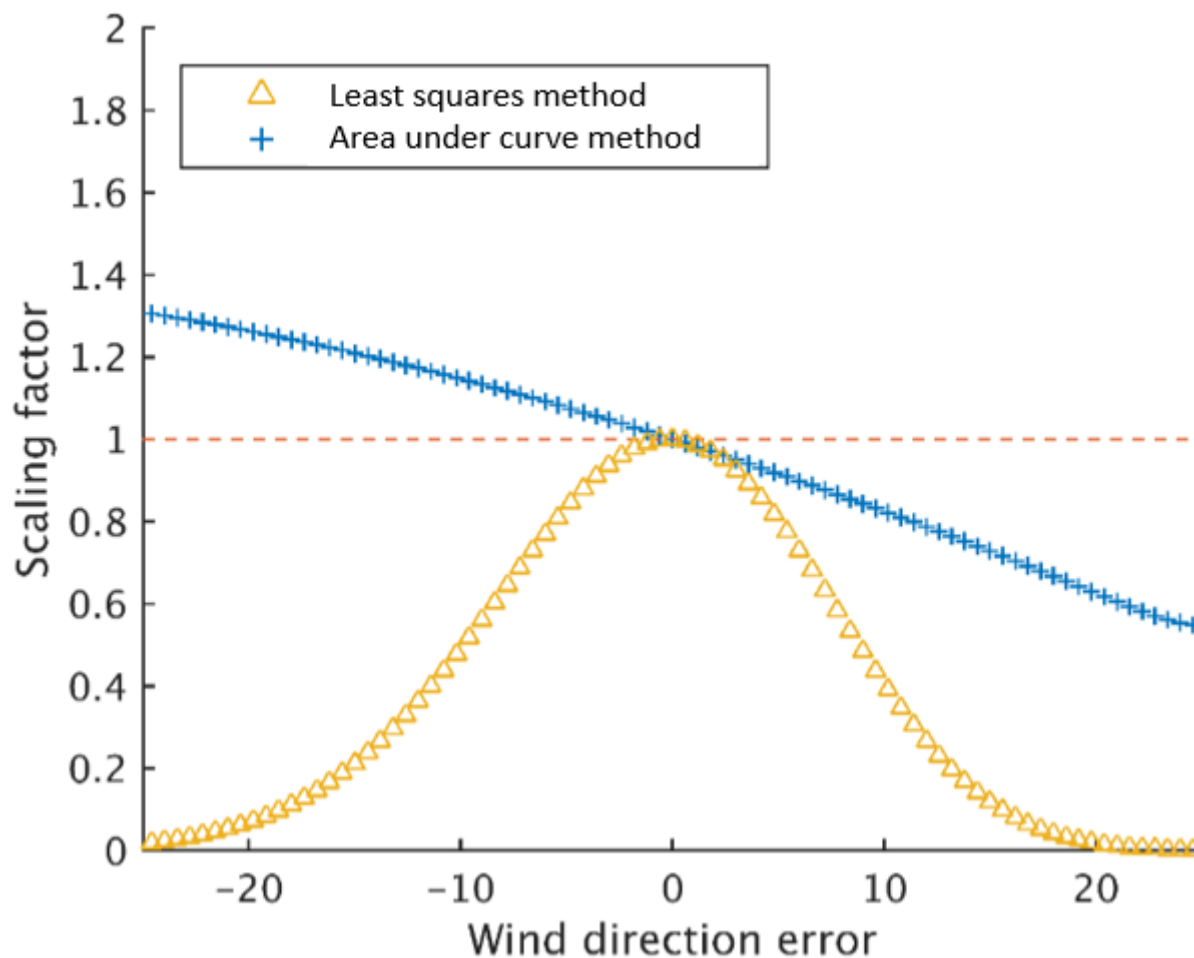


Figure 16: A demonstration of the effect of model transport error on the optimized emission rate using pseudo-observations transecting a modelled plume at a 45° angle. The scaling factor represents the change in the optimized emission rate compared to the true emission rate, with 1 representing a perfect rate.

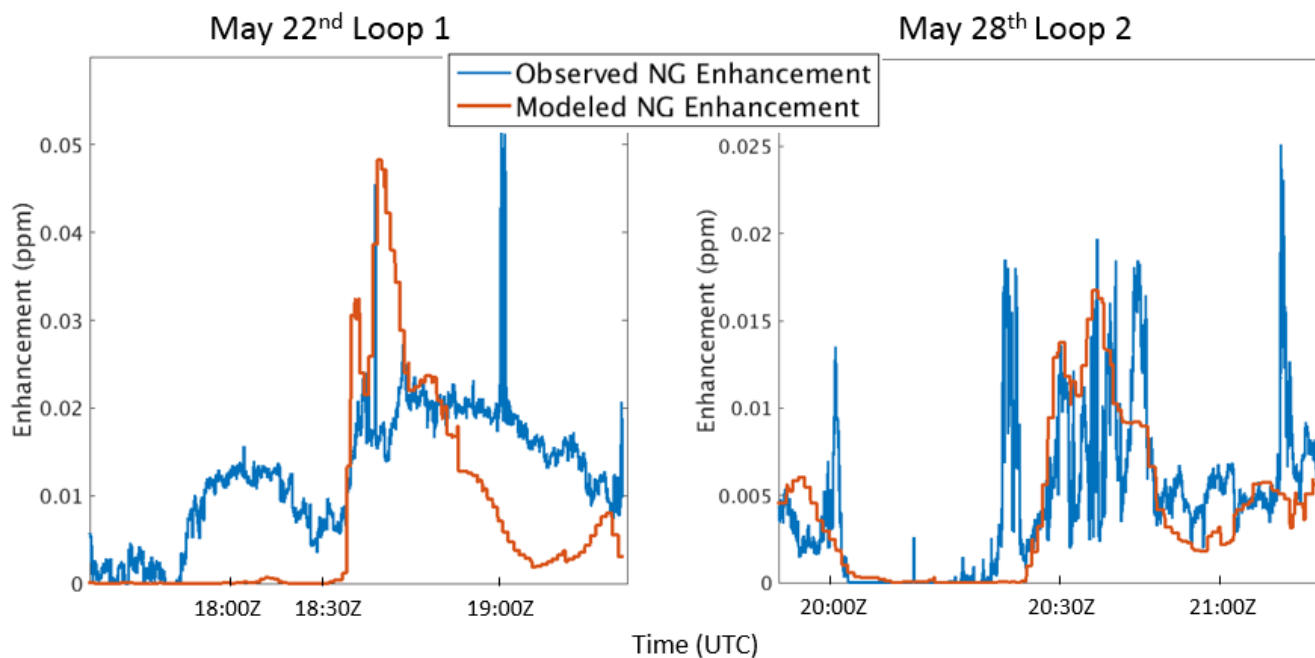


Figure 17: Comparison of observed natural gas enhancement to modelled natural gas enhancement for segments along the (left) May 22nd flight and (right) May 28th flight. A distinct lack of representativeness of the observations in the modelled enhancement can be seen in the May 22nd flight compared to the May 28th flight.

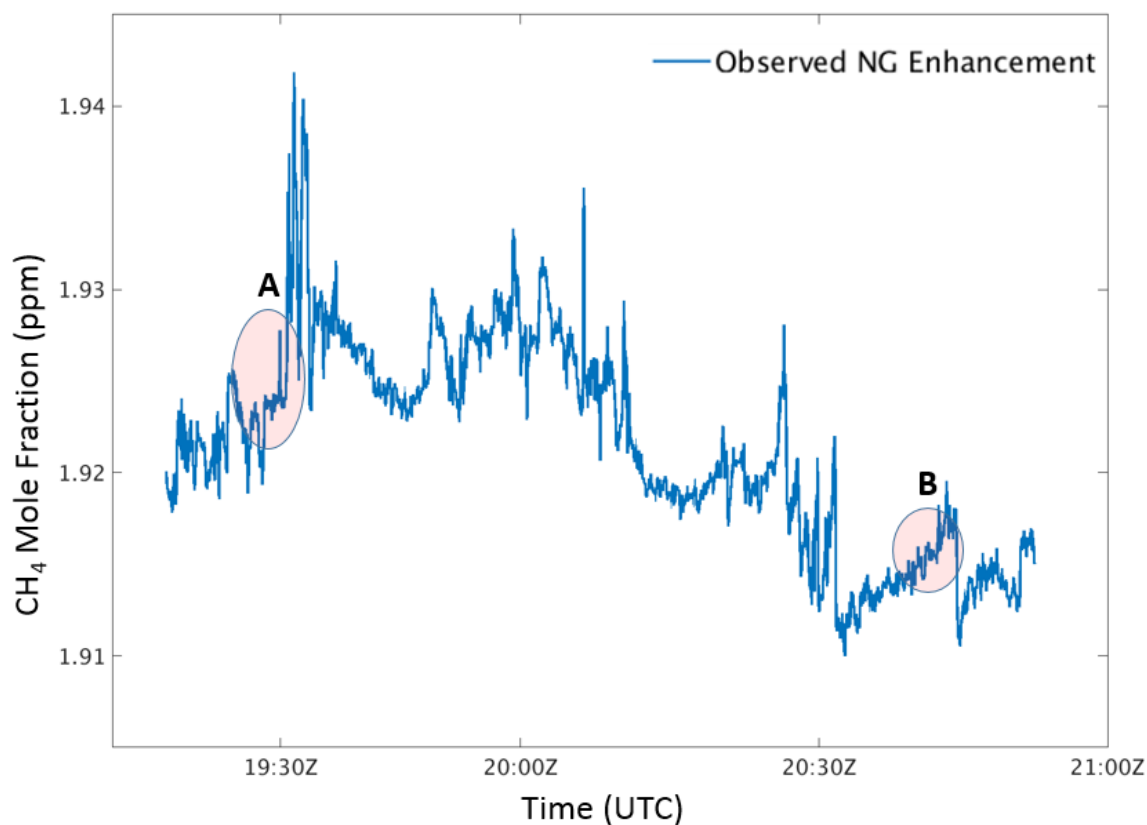


Figure 18: Time series of CH₄ mole fractions from the second loop of the May 22nd flight. Observations at the shaded areas below A and B were taken at similar locations in space, showing the change in the background mole fraction across time.

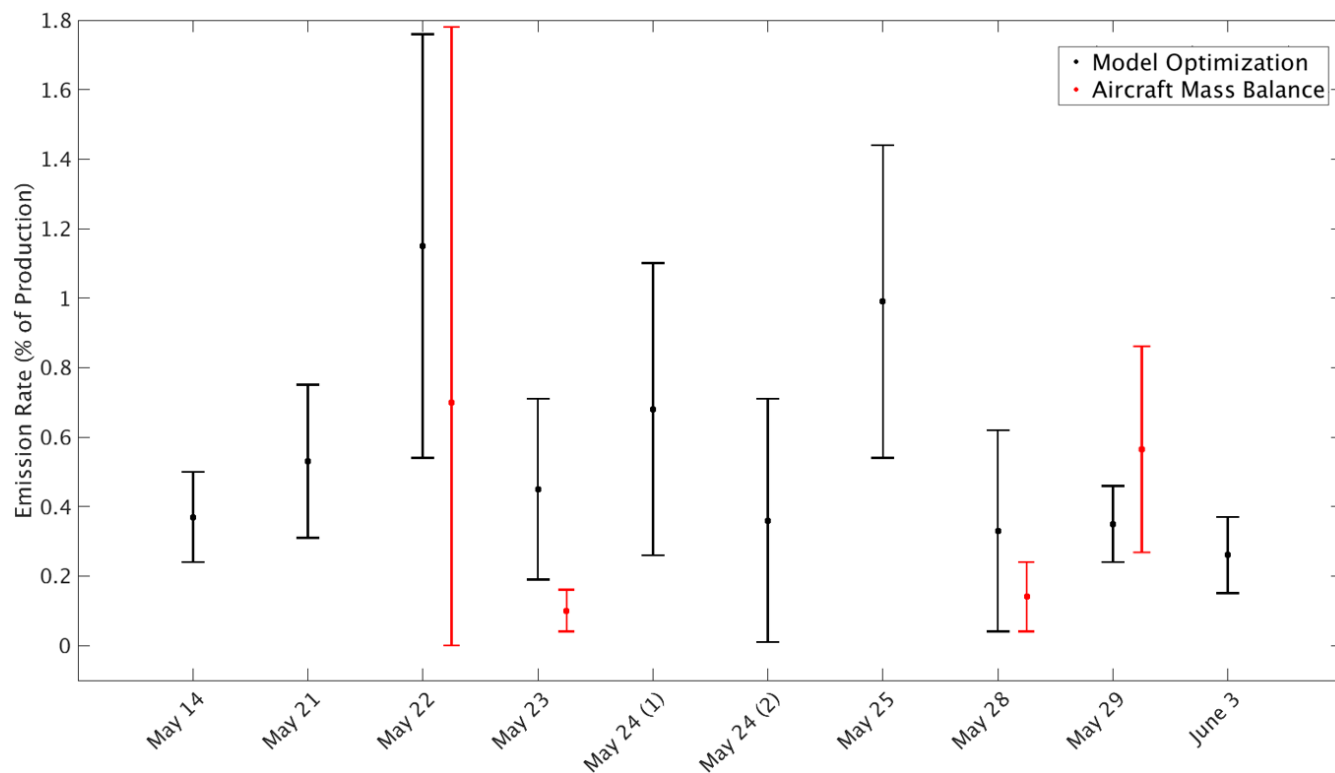


Figure 19: Calculated upstream natural gas emission rates using (black) model optimization technique and (red) aircraft mass balance technique.

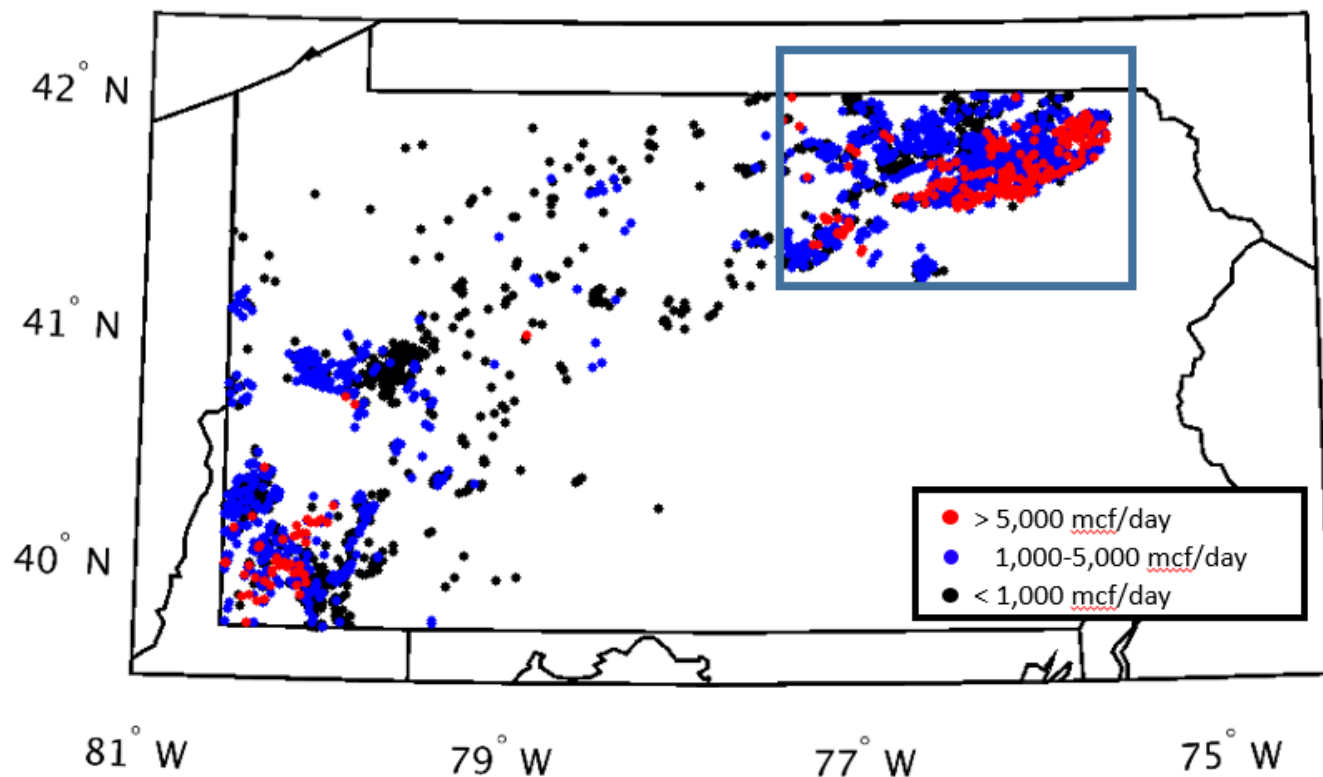


Figure 20: Well locations and daily production of unconventional wells in PA for May 2015. Boxed region is study region where flights took place.

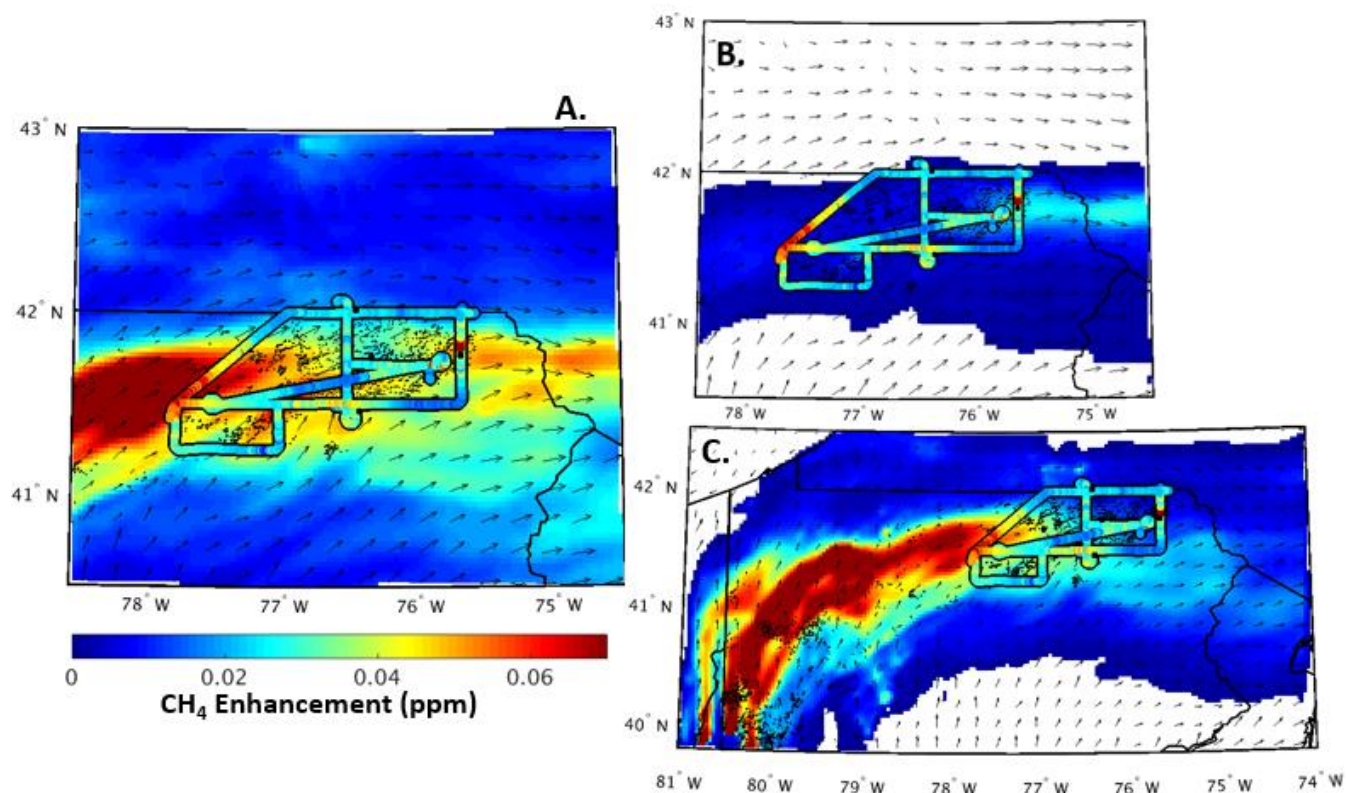


Figure 21: Observations vs modelled enhancements of the flight from Peischl et. al (2015) for July 6th, 2013. (a.) Observed enhancements from the flight over model projected enhancements from all sources at 21Z. (b.) Projected enhancement from upstream gas processes using a 0.4% emission rate. (c.) Projected enhancement from coal sources in southwestern PA.